

The Source Parameter of S1222a Marsquake obtained from Spectral Analyses using Empirical Green's Function

Taichi Kawamura¹, Zongbo Xu², Wanbo Xiao¹, Ludovic Margerin³, Sabrina Menina⁴, Philippe Lognonné⁵, and William Bruce Banerdt⁶

¹Université Paris Cité, Institut de physique du globe de Paris, CNRS

²Universite Paris Cite, Institut de Physique du Globe de Paris

³IRAP/CNRS

⁴Université Paris Cité, Institut de Physique du Globe de Paris

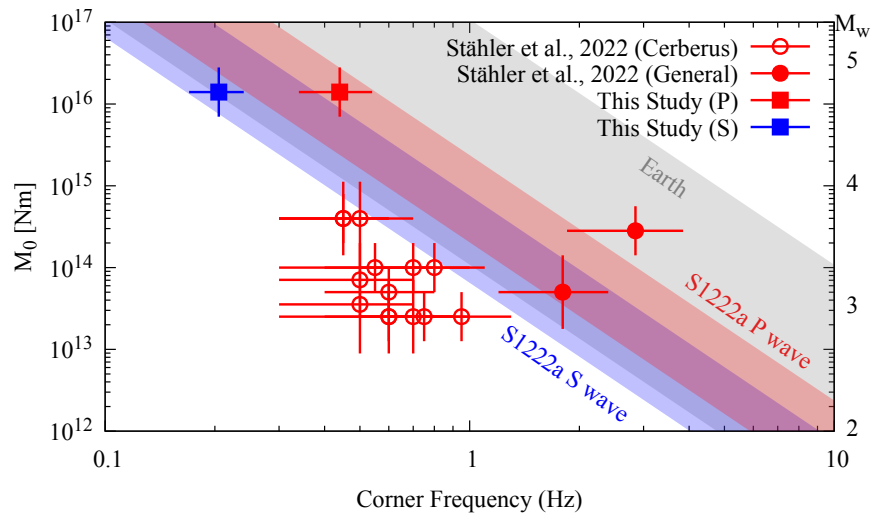
⁵Université Paris Cité, Institute de physique de globe de Paris, CNRS

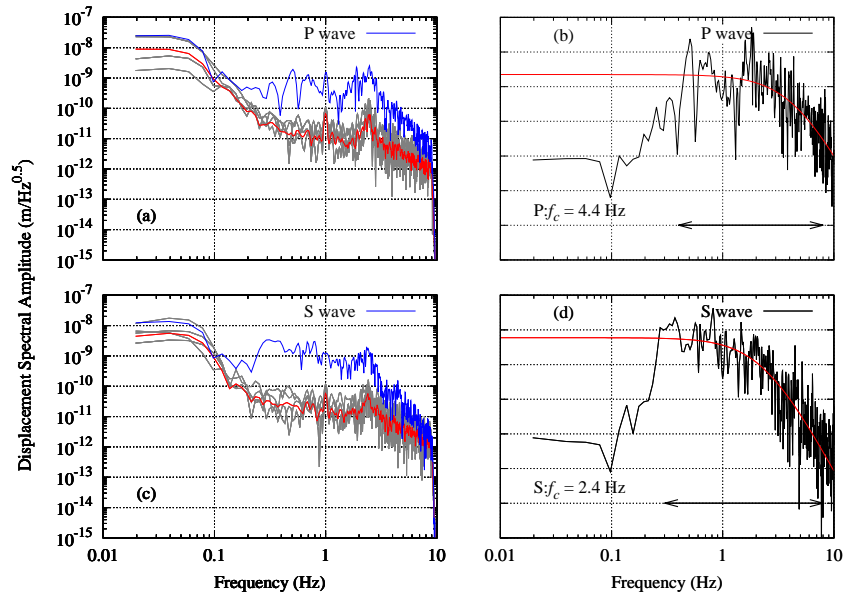
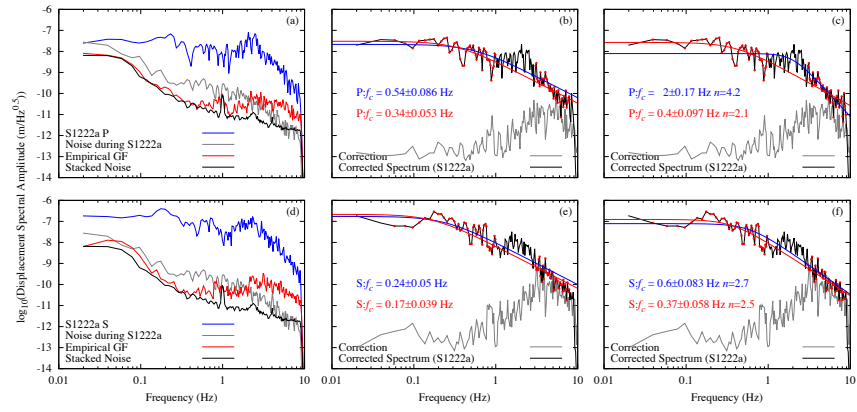
⁶Jet Propulsion Laboratory, California Institute of Technology

March 26, 2023

Abstract

NASA InSight mission revealed that Mars is seismically active today and identified a region with high activity called Cerberus Fossae. Since then, the origin of marsquakes has been an important question in Mars seismology. On 2022/05/04, InSight seismometer detected the largest marsquake during the mission, named S1222a. The source was estimated to be outside the Cerberus Fossae and it would be important to constrain the source parameters of this remarkable event. In this study, we estimate the source parameters of S1222a through spectral analyses. Since we found that seismic spectra of S1222a are heavily contaminated, we performed Empirical Green's Function analyses. We found that the corner frequencies are 0.34-0.54 Hz for the P wave and 0.17-0.24 Hz for the S wave. These values are slightly higher than those of seismic events at Cerberus Fossae, which implies a faster rupture at the source and different origin for S1222a.





The Source Parameter of S1222a Marsquake obtained from Spectral Analyses using Empirical Green's Function

Taichi Kawamura¹, Zongbo Xu¹, Wanbo Xiao^{1,2}, Ludovic Margerin³, Sabrina Menina¹, Philippe Lognonné¹, William Bruce Banerdt⁴

¹Université Paris Cité, Institut de physique du globe de Paris, CNRS, Paris, France

²Department of Geophysics, School of Earth and Space Sciences, Peking University, Beijing, China

³Institut de Recherche en Astrophysique et Planétologie, Toulouse, France

⁴Jet Propulsion Laboratory, California Institute of Technology, CA, USA

Key Points:

- We performed spectral analyses of the largest marsquake S1222a to constrain its source parameters.
- We used Empirical Green's Function to improve our analyses and separate the effect of attenuation and the source parameters.
- The corner frequencies we obtained for S1222a indicates faster rupture compared to marsquakes at Cerberus Fossae and implies a different source mechanism.

Abstract

NASA InSight mission revealed that Mars is still seismically active today. Since then, where and how marsquake occur has been one of a key questions martian seismology. InSight also found that Cerberus Fossae region, about 1500 km east from InSight landing site, is seismically active with numerous marsquakes occurring in this region. On the other hand, on 2022/05/04, InSight seismometer detected the largest marsquake during the mission, named S1222a. The source was estimated to be outside the Cerberus Fossae and it would be important to constrain the source parameters of this remarkable event. In this study, we estimate the source parameters of S1222a through spectral analyses. We mainly focus on the corner frequency since it will help us better understand the rupture process of the seismic event. However, we found that seismic spectra of S1222a are heavily contaminated, which makes it difficult to constrain the spectral features. Thus, we took the approach of Empirical Green's Function to correct for the contamination. This successfully corrected the observed spectra which enabled us to constrain the source parameters by fitting the model source time function to the observed spectra. We found that the corner frequencies are 0.34-0.54 Hz for the P wave and 0.17-0.24 Hz for the S wave. These values are slightly higher than those of seismic events at Cerberus Fossae, which implies a faster rupture at the source. This implies that S1222a has different origin compared to typical events at Cerberus Fossae.

Plain Language Summary

NASA InSight mission revealed that Mars is seismically active today and identified a region with high activity east to InSight landing site called Cerberus Fossae. Since then, the origin of marsquakes has been an important question in Mars seismology. On 2022/05/04, InSight seismometer detected the largest marsquake (S1222a) during the mission and interestingly, this occurred outside the Cerberus Fossae. In this study, we used Empirical Green's Function analyses to study the spectral feature of this remarkable event. Through the spectral analyses, we found that the rupture speed of S1222a is faster compared to typical events from Cerberus Fossae. This implies that S1222a has different type of seismic source compared with those of Cerberus Fossae.

1 Introduction

NASA InSight (Interior Exploration using Seismic Investigations, Geodesy and Heat Transport) mission has opened a new field of martian seismology since its landing on Mars in 2018 (Banerdt et al., 2020). InSight SEIS instrument (Lognonné et al., 2019) performed a quasi-continuous observation of martian seismicity from early 2019 to middle 2022. The almost 4 years of seismic monitoring of the planet, revealed Mars as seismically active and the seismic events were used to deepen our knowledge of the internal structure of the planet (Lognonné et al., 2020; Giardini et al., 2020; Knapmeyer-Endrun et al., 2021; Khan et al., 2021; Stähler et al., 2021; Drilleau et al., 2022; Durán et al., 2022). Among the various questions addressed by InSight are those related to the distribution of seismic activities and the source mechanism of marsquakes. InSight observations revealed Cerberus Fossae, a region located about 1500 km east to the landing site, as seismically active today with about half of the marsquake detected (Giardini et al., 2020). Furthermore, moment tensor analyses of major seismic events of this region showed that the source mechanism of events are consistent with the direction of the fault system in the region (Brinkman et al., 2021; Jacob et al., 2022). In addition to the source mechanism, there were also efforts to constrain the source dynamics, including rupture time or source cutoff-frequency of these events (Stähler et al., 2022). Constraining source parameters of marsquakes will help us in understanding the rupture process of martian seismicity and the dynamics inside the planet. While such studies were made for the Cerberus Fossae region, we still have little constraints of events outside this region.

On 2022/05/04, the largest marsquake during the InSight observation, known as S1222a, was detected by the InSight SEIS instrument (Kawamura et al., 2022). Its moment magnitude was 4.7 and the event had remarkably high S/N over wide frequency band from 1/30 Hz to 35 Hz. Such a broad band seismic signal allow constraining the source parameter of this event through spectral analyses. One way to describe seismic spectra is to express this with a source time function and an attenuation term.

$$A(f) = \frac{\Omega_0}{1 + (f/f_c)^2} \times \exp\left(-\frac{\pi ft}{Q}\right) \times R(f) \quad (1)$$

where f_c is the corner frequency, Ω_0 is the DC spectrum (zero-frequency spectrum) amplitude, Q is the attenuation quality factor, t is the travel time and $R(f)$ is a frequency dependent amplification term related to crustal structure and layering which include side effects. The first term is the source time function known as ω^2 model, which is a model that explains well the double couple source observed on the Earth (Aki & Richards, 2002). The second term is the attenuation, which should be regarded as an effective attenuation including both the scattering and absorption. Ω_0 and f_c provide us with some key source parameters, such as seismic moment, rupture duration, or stress drop which is an essential piece of information to understand the dynamics of the seismic source. The last term however can hide the frequency signature of the source. This is especially true for stations located on complex crustal and subsurface layering, such as those found for InSight from Receiver Function analyses (Lognonné et al., 2020; Knapmeyer-Endrun et al., 2021; Shi et al., 2023) and subsurface inversions Hobiger et al. (2021); Kenda et al. (2020); Carrasco et al. (2023).

Such model was successfully applied to terrestrial, lunar and martian quakes to constrain their source parameters (e.g. Allmann & Shearer, 2009; Kawamura et al., 2017; Stähler et al., 2022) and thus it will be a natural path to apply this to S1222a spectrum to understand its source parameters. We first describe the data used (Section 2), describe the general characteristics of the seismic spectra and point out some atypical observed features (Section 3). Then we describe the Empirical Green’s Function Method (EGF) used in this study to deal with such atypical features and to better constrain the source parameters. After validation with a test case, we provide our main results with S1222a (Section 5). Finally, We conclude by discussing possible implications on the origin of S1222a as well as perspectives for future spectral analyses with InSight data in Section 6.

2 Data

We used the waveform data of InSight Very BroadBand (VBB) seismometer (InSight Mars SEIS Data Service, 2019a,b), the high sensitivity broadband seismometer of InSight mission (Lognonné et al., 2019). During the event, this was the only sensor operating, due to power constraints. No environmental (Banfield et al., 2019) nor short-period seismic sensor (Lognonné et al., 2019) data are therefore available. Although 100 sps VBB are available at the time of the event, we focus our analysis on the DC-10 Hz bandwidth. Above this bandwidth and especially for our EGF analysis, for which other marsquakes are used, most of the periods have indeed no 100 sps VBB channels but only 100 sps SP channels. As the instrument responses of the VBBs and SPs are imperfectly known at high frequency, including due to rotation effects of SEIS on the weakly consolidated Mars surface (Fayon et al., 2018), the use of different sensors might indeed generate errors in the determination of the site effect function $R(f)$. The data were rotated to ZRT component with the back-azimuth presented in Kawamura et al. (2022). Event parameters (e.g. location, time, magnitude) are those published by the Marsquake Service (MQS) (Clinton et al., 2018) in V13 catalog InSight Marsquake Service (2023) and Kawamura et al. (2022). We searched in the catalog events with similar epicentral distances with S1222a to estimate the EGF. To obtain the spectra, we use the P and S spectral windows given in the MQS catalog, as well as the noise window. A Time window

duration of 30 second was used to avoid the effect of scattered or converted wave that may contaminate our analyses.

3 Spectral Features of S1222a Spectrum

We first review the general spectral feature of S1222a. Figure S1 shows the P and S spectra of S1222a calculated from 100 Hz data with 30 second time window on the vertical component. The pre-event noise is also plotted for comparison. As Kawamura et al. (2022) point out, the seismic signal significantly exceeds the noise from about 1/30 Hz to 20 Hz for P wave and up to 35 Hz for S wave. Another characteristic feature of the spectra is the broad peak observed above 1 Hz. The characteristic peak around 2.4 Hz is a well known feature observed regularly in InSight data (Ceylan et al., 2021; Dahmen et al., 2021). For S1222a, we see that the energy is enhanced much wider in frequency as shown in Figure S1. Such feature was not as obvious for previous marsquake records, except for the 2.4 Hz peak. This is likely due to the high S/N of S1222a that enlightens the effects not visible with previous events at high frequencies.

A straight forward way to constrain the source parameter is to fit the spectra with the model described with Eq. 1. To avoid the trade-off between the corner frequency and the attenuation factor, we fixed the Q to the value used by Stähler et al. (2022): $Q_P = 2250$, $Q_S = 1000$ without frequency dependency. We tested two fittings, in the 0.05 Hz-20 Hz and 0.05 Hz-0.9 Hz bandwidth respectively. The first takes the full band width with sufficient S/N and the second excludes the 2.4 Hz peak. In both cases, we were not able to find reasonable solutions. For the first case, we were able to find a reasonable fit for the P wave but the obtained corner frequency by far exceeds the frequency band used ($f_c = 3172$), meaning a full explanation of the spectrum by attenuation. On the other hand, we were not able to find a reasonable fit for S wave with the reference Q value. The model decays faster than the observation. The second fit's setting with limited frequency band gives better fit for both P and S waves. However, the deviation between the model and the observation is large at higher frequencies and the model cannot explain the observed spectra. It is also worth noting that we found higher corner frequency for P wave with respect to S wave, which contradicts what is theoretically predicted (Sato & Hirasawa, 1973; Madariaga, 1976). To further investigate the spectral characteristics, we conducted fittings with various Q values varying from $Q = 1000-6000$ (Figure S2;S3). The broadband fittings favor extremely high corner frequencies. The narrow band fittings give reasonable fit but the spectra can be fitted with wide ranges of Q and f_c due to the lack of information of high-frequency decay which is completely masked with the broadband peak at 2.4 Hz.

In all cases, the fittings do not give us reasonable results. This strongly suggests that the excess of energy in the high frequency is an additional effect that contaminates the seismic spectra and/or that the attenuation models are not valid for the S1222a path. Such complex attenuation structure can also be seen from evolution of coda shapes (Figure S4). These points need to be taken into account when performing spectral analyses. Such discrepancy between the model and the observation reinforce the importance of the site effect at the InSight landing site. It is well known that the subsurface structure below the station can generate some characteristic reverberations that can result in such site effect (Towhata, 2008). While a modeling approach to evaluate the site effect is possible (Xiao et al., 2023), we prefer in our approach to overcome this problem by using EGF analyses.

4 Method: Empirical Green's Function Analyses

Empirical Green's Function analyses were first proposed by Hartzell (1978). The main idea of this method is to use small aftershocks events which occurred close to a larger event of interest as the Green's Function of this event, given that all events propagate

in the similar path and experience similar propagation effects, including attenuation, scattering and local effects such as site effects. By deconvolving a seismic spectrum with EGF, we obtain the source time function component observed in the spectrum. This is a powerful tool to remove the contamination from seismic spectra as it requires no hypothesis on the propagation properties. Through the EGF analyses, we expect for S1222a to be able to remove the site effect contamination observed at higher frequencies, as well as attenuation unknown and can therefore perform a much better estimation of the spectral feature and the source parameters.

First, we tested our approach with another event, the S1094a event, which we consider as a possible reference. S1094a is a large impact, equivalent to a magnitude of about 4 and its source parameter were discussed in seismological and in impact physics' points of view (Posiolova et al., 2022), leading to a source time function well constrained. Note however that Garcia et al. (2022) and Posiolova et al. (2022) both proposed that the impacts' source time function decays in cube and not in square. Thus, after we correct the spectra with the EGF obtained by stacking the smaller events, we fit the data with ω^3 model and show results on Figure 1. The S1094b raw spectra are shown in blue in Figure 1 (a) and (c). It is worth pointing out that the peak at 2.4 Hz is also visible here but is not as broadband as it was observed in S1222a. The red line in Figure 1 (a) and (c) is EGF obtained from the stack of smaller events with similar distances. Stacking is one of the common methods used to improve S/N for EGSs (Prieto et al., 2004; Shearer et al., 2006). For this stack, we used MQS catalog (InSight Marsquake Service, 2023) and picked up all the events with Quality A and B, which have relatively good constraints on the epicentral distance (see Clinton et al. (2021) for detailed description of the quality). We used $t_s - t_p$ as a measure of distance to avoid the dependency of the distance with the internal structure and took all events having their $t_s - t_p$ within 25 seconds to the $t_s - t_p$ value of the selected event. The impact of the choice of the threshold magnitude is shown in Figure S5. The impact is minor and 25 second provides a sufficient number of events to obtain EGF. The list of events used in the analyses can be found in Table S1. Figure 1 (b) and (d) shows the result of the correction and the fitting. We can already see in the figure that the correction successfully removes the peak at 2.4 Hz and makes the form of the spectra closer to typical ω^3 model. The decay at the lower frequency is due to the loss of S/N towards low frequencies. We found a corner frequency of 4.4 Hz, which is higher than the 3 Hz corner frequency proposed in Posiolova et al. (2022). Such slightly larger frequency still matches values expected from impact physics described in Posiolova et al. (2022). We also found the corner frequency for S wave to be 2.4 Hz, which provides a frequency ratio of 1.8, close from the expected ratio of V_p to V_s seismic velocities. While how impacts excite S wave will need further discussion, we found a lower corner frequency for S wave than P wave, as proposed for quakes by classic theories (Sato & Hirasawa, 1973; Madariaga, 1976). These results give reasonable results that agree well with previous results and thus encourage us to move forward to the analyses of S1222a.

For S1222a, the challenge is to obtain a reasonable EGF. One of the key features of S1222a is that it has high S/N among wide frequency band that was never seen for any of the marsquakes detected before. Marsquakes are classified with their frequency content and LF/BB type events have typically energy at frequencies lower than 2.4 Hz while HF/VF type events mainly have energy at 2.4 Hz or higher (Clinton et al., 2021). This is critical to the EGF analyses since the frequency band that we can use in the analyses depend on the frequency band we can define our EGF. To obtain an EGF that is suitable for correcting the wide frequency band of S1222a, we used weighted stack with different types of marsquakes. The weight was calculated using the S/N for each frequency and the stacked spectrum can be expressed as

$$G(f) = \frac{\sum_i \frac{|S_i(f)|}{|N_i(f)|} S_i(f)}{\sum_i \frac{|S_i(f)|}{|N_i(f)|}} \quad (2)$$

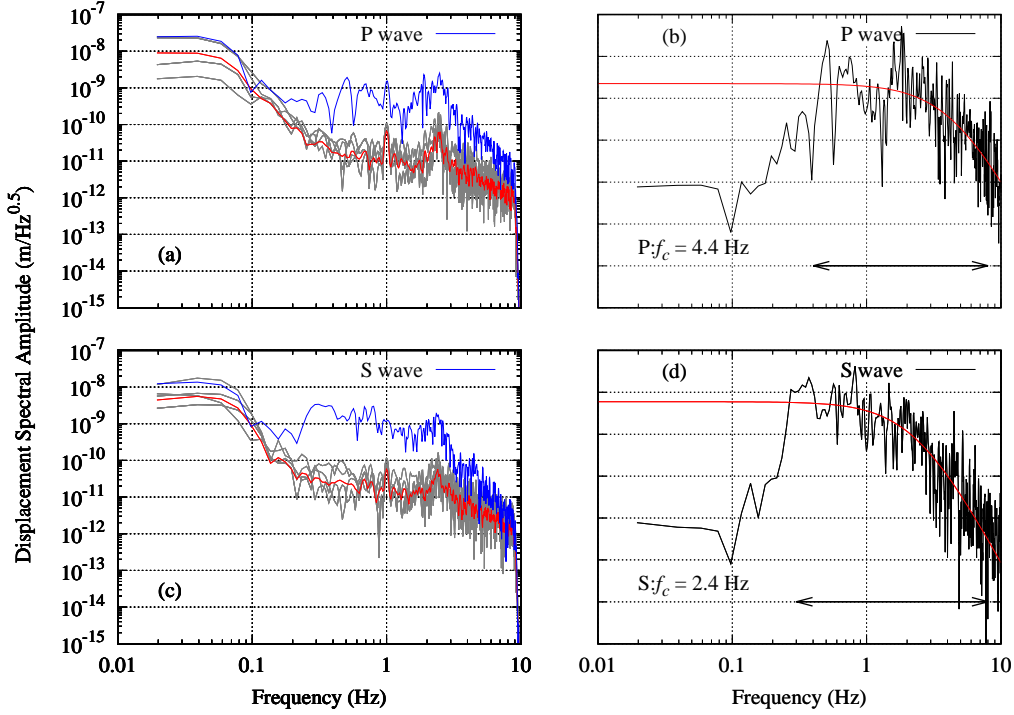


Figure 1. EGF analyses performed for S1094b. (a), (c): The results for P and S waves respectively. We show all the spectra used in the analyses. The blue line is the original spectrum of S1094b and the gray lines are all the spectra used to estimate the EGF. The red line is the EGF which was obtained by stacking all the black spectra. (b), (d): Corrected spectra with the result of the fitting. The corrected spectra is shown in black and the red line on the right panel is the fitted spectra using ω^3 model following the discussion from Garcia et al. (2022); Posiolova et al. (2022).

$G(f)$ is the EGF we obtain. $S_i(f)$ and $N_i(f)$ is the spectral energy for signal and noise spectra at frequency f for i th event. By weighting the stack, the high frequency component of the EGF is mainly constrained by VF and HF events whereas the low frequency component is constrained with LF and BB events.

Before performing the stack, all the spectra were resampled to be linear in logarithmic scale and to smooth the spectra. The data were resampled to from 10^{-2} to 10^2 Hz with 0.1 increment for the power. We took the same criteria for the event selection as used for S1094b. Among these events, we excluded those with a magnitude larger than 3.0 to minimize the influence of corner frequencies of the stacked event to the EGF. While we would like to have low magnitude events to avoid the contamination of the source time function in the EGF, we also need events with enough S/N to obtain a meaningful EGF. This requires us to take a magnitude of 3.0 as the threshold (Figure S6). This will leave us with 13 events listed in Table S2.

5 Results

In Figure 2, we show our results of the EGF analyses on the vertical components. Results for the other components are in the supplementary information (Figure S7,S8).

If we focus on the EGF spectra and the stacked noise spectra (blue and black lines in the Figure 2 (a),(c)), we see that below 0.5-0.6 Hz the two spectra almost overlap. This means that our EGF is already contaminated by the noise in this frequency band. Thus, in order to not contaminate the seismic spectra with noise, we removed the noise energy from the EGF by deconvolution and obtained a correction spectrum as shown in Figure 2 (b),(d) (in gray). We see that the correction spectra are flat at low frequencies but well represent the energy enhancement at high frequencies. Then we correct the S1222a spectra with the correction factor and we obtain the spectra shown in black in Figure 2 (b),(d). We still see some residual of the 2.4 Hz peak but the overall shapes of the spectra are improved. Then we fit the curve with the ω^2 model using the least square method in 0.05 – 8 Hz to obtain the corner frequency. The result of the fit is shown in Figure 2 (b),(d). The fittings seem to be good up to 5 Hz despite of the small residual of the site effect. At higher frequencies, the misfit however increases. To test if the observed misfit is due to residual of the 2.4 Hz energy, we performed additional fits by excluding the values between 1–3 Hz. The fit at high frequencies seem to be better, but with minor improvements. The obtained corner frequencies are 0.34-0.54 Hz for the P wave and 0.17-0.24 Hz for the S wave and in both cases, the frequency range corresponds to the 1 σ error from the fitting. When we compare the results from different components, the results are stable for S wave ranging from 0.17-0.32 Hz, while for P wave we found some higher values on the transverse component (0.66-0.87 Hz). This might be due to the lower S/N on the transverse implying that the residuals of the 2.4 Hz have larger effect on the fit. Interestingly, we find values significantly smaller for the S wave, which was not the case when we estimated corner frequencies with raw spectra (Figure S1). Similar results were also seen for S1094b, which might imply that this is a feature that was enlightened due to the correction with EGF, demonstrating the importance for site effect corrections.

6 Discussion

6.1 Corner Frequency and Implication for the Origin of S1222a

The corner frequency we found for S1222a is relatively high compared to those found for other events by Stähler et al. (2022) for the Cerberus Fossae. The higher corner frequency will result in a higher stress drop and from the values that we obtained, and we find a stress drop of 0.1-0.7 MPa with the parameter used in Stähler et al. (2022) (3 km/s for β and $k = 0.38$ for P wave, and $k = 0.26$ for S wave). This is also consistent with results found by theoretical study in Xiao et al. (2023) 3. S1222a has therefore a stress drop comparable to those of Earthquakes, in contrary to those of Cerberus Fossae, found with significantly lower than 0.1 MPa stress drop. Stähler et al. (2022) attributes the low stress drop in Cerberus Fossae region to a structurally weak, potentially warm source region resulting from recent volcanic activity. The location of S1222a (Kawamura et al., 2022), 820 km away from the one of S0235b in Cerberus Fossae region (Clinton et al., 2021) and closer from the Mars dichotomy, suggests therefore important lateral variations in term of seismogenic properties. If these are related to the seismogenic temperature and the later are correlated with a possible mantle plume beneath Elysium (Broquet & Andrews-Hanna, 2023), S1222a location appears indeed further. Another interesting feature of the corner frequencies we found is that we found lower corner frequency for S wave with respect to P wave. This is predicted in theoretical studies Sato & Hirasawa (1973); Madariaga (1976) and we have typically corner frequency of P wave higher by a factor of about 1.5. However, our results suggest that the ratio is about 2. This implies that the apparent pulse duration is longer for S wave. Such a difference may be observed due to, for example, the characteristics of the fault or geometrical settings between the source and the station. Further investigations are needed to understand the observation better and it will be important to obtain the source parameters of more marsquakes to have a more statistical view on this aspect.

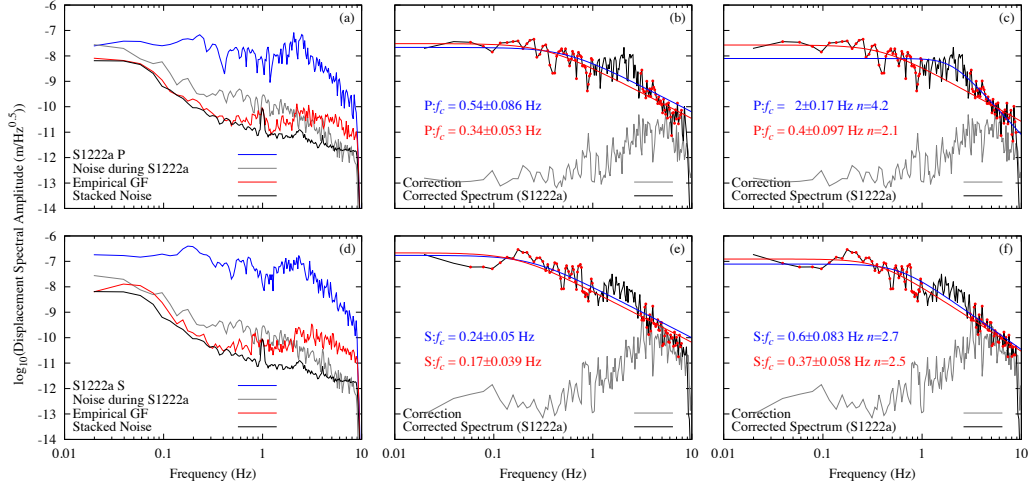


Figure 2. Empirical Green’s Function (EGF) analyses performed for S1222a on the vertical component. The top and the bottom panels show the results for the P and S waves respectively. On the panels (a) and (d), we show the signal and noise spectra of S1222a and EGF. The blue and the red lines show the S1222a and EGF spectra, respectively. The gray line is the noise level during the S1222a event and the black line shows the stacked noise obtained from noise spectra of different events used to estimate EGF. On the panels (b), (c), (e) and (f), we show the corrected spectra for S1222a with EGF. The black line is the corrected spectra and the gray line is the correction spectra that was used to the correction. The correction spectra were obtained by correcting EGF with stacked noise spectra. The red dots are the data used for the fit after excluding the data in $1 - 3 Hz$. On the panels (b) and (e), the blue and red curves are the results of the fits using ω^2 model Aki & Richards (2002) for all data and data without $1 - 3 Hz$ data, respectively. On the panel (c) and (f) we used generalized form of the source time function (Abercrombie, 1995) and the fit with the full data is shown in blue lines and the red lines are fitted to data without $1 - 3 Hz$ data. The results of the fits are shown in the corresponding colors.

6.2 Spectral Decay of S1222a

Following previous studies (Allmann & Shearer, 2009; Stähler et al., 2022; Kawamura et al., 2017), we fixed the source time function to the ω^2 model. However, it is possible that the source time function may be different for S1222a given the different tectonic content for this event. Thus, we introduce here more general form of the source time function expressed as

$$A(f) = \frac{\Omega_0}{(1 + (f/f_c)^\gamma)^{\frac{1}{\gamma}}} \quad (3)$$

(e.g. Abercrombie, 1995; Shearer, 2019). γ depends on the choice of the source model and $\gamma = 1$ when we follow the model of Brune (1970) or $\gamma = 2$ when we follow the model of Boatwright (1980). n is the parameter that defines the spectral decay. To test whether these models explain better the observed spectra by fitting the data with 3. We tested both $\gamma = 1$ and $\gamma = 2$ and all the results are shown in the supplementary information. In Figure 2, the results for the vertical component with the model using $\gamma = 1$ is shown. Given the larger degree of freedom, the influence of the residual of the 2.4 Hz peak becomes more problematic here and we see that for the P wave, the model fits the 2.4 Hz peak instead of the seismic spectrum. On the other hand, the fit is further improved when we removing data $1 - 3 Hz$ and we found $n = 2.1$. This is not so differ-

ent from the ω^2 model but we see slight improvement for the fit at the highest frequencies. For the S wave, we found clear difference from the original results and $n = 2.5-2.7$, which is significantly different from the ω^2 model. We also see that the fit is improved especially at high frequencies. This strongly supports the idea that the spectral decay for S1222a significantly differs from ω^2 model. Also with other settings with different γ and different components, we found similar results for S wave with $n = 2.3-3$ (Figure S7-S11). This confirms the the decay of the S1222a spectrum significantly differ from the classical ω^2 model. Such deviations from the ω^2 model are common in dynamic simulations of simple sources (Kaneko & Shearer, 2014). They have also been reported in several studies on Earth (e.g. Eulenfeld & Wegler, 2016; Uchide & Imanishi, 2016; Eulenfeld et al., 2021). What such deviation implies is still an open question. As shown in Kaneko & Shearer (2014), it is possible to fit the same dynamic model of the source with different empirical forms of the source spectrum. Proposed possibilities can vary from the geometrical settings and the shape of the fault (Shearer, 2019), heterogeneity on the fault surface and incoherent slip (Uchide & Imanishi, 2016), and/or magnitude dependency of the source time function (Eulenfeld & Wegler, 2016). Non of them are conclusive and it is not yet clear how they can be applied to martian condition. Further investigations are needed and it would be important to keep in mind such deviations in future works.

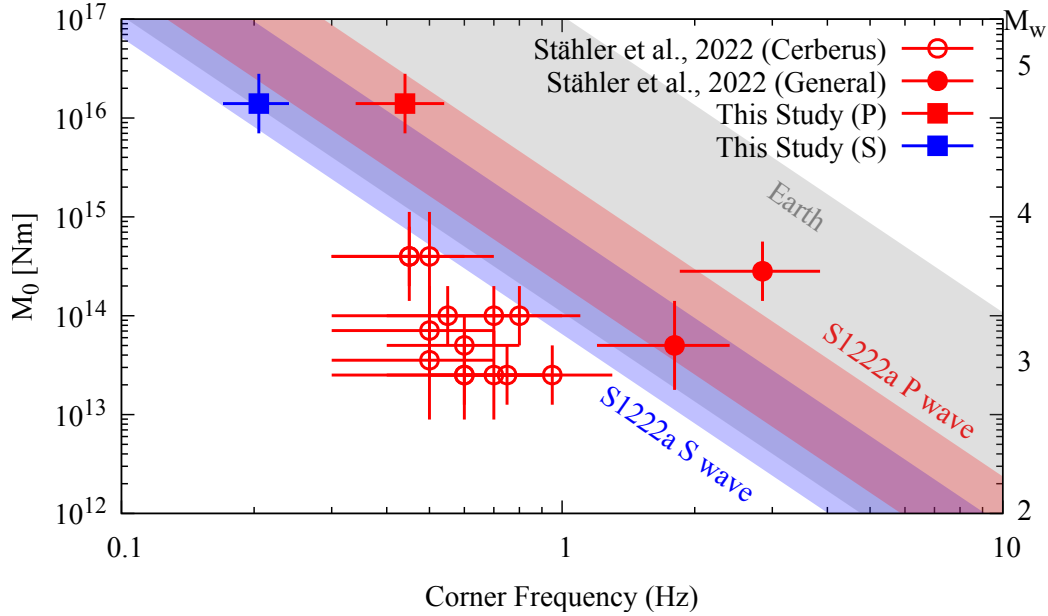


Figure 3. Scaling Relationship between corner frequencies and seismic moment. The red and blue shaded area shows the range of acceptable values from this study. The boxes are the values from this study. The circles are the results from Stähler et al. (2022). The open circle is the values obtained for seismic events in Cerberus Fossae region and the filled circles are those outside the region. Typical scaling relationship for Earth is shown as gray shaded area.

6.3 Implication for the Possible Contamination in Seismic Spectra and Empirical Green’s Function Analyses

This study demonstrated clearly that there is a significant contamination at high frequency of seismic signal that masks the true spectral feature. One possibility for the source of such contamination will be the site effect excited by the local structure around the InSight lander (Carrasco et al., 2023). Xiao et al. (2023) investigates this more in

detail by theoretically evaluating the effect of subsurface structure to the observed spectra. It is worth mentioning that while we succeeded in obtaining corner frequency for S wave, the theoretical approach taken by Xiao et al. (2023) had difficulty in explaining the observed S spectrum. This might be implying that there is some phenomena that was not taken into account in the theoretical investigation but was included in the EGF. This might be a clue to better understand the origin of the site effect and contamination in seismic spectra.

It is also important to note that it is very likely that this effect is seen for many of the marsquakes that were observed before, especially for VF/HF events and part of BB events (Carrasco et al., 2023). The main feature of the contamination we observed in this study was the enhancement of energy above 1 Hz centered at 2.4 Hz. Therefore, all events that have significantly energy above 1 Hz may have been influenced by such contamination. This point needs to be taken into account when performing spectral analyses of InSight data.

7 Summary

In this study we investigated the spectral feature of the largest marsquake S1222a to constrain its source parameters. We found that the seismic spectra were significantly contaminated at higher frequencies and thus we performed EGF analyses to correct for this. The correction made through EGF analyses successfully retrieved the main feature of the seismic spectra. We were able to obtain the corner frequency of P and S waves as 0.34-0.54 Hz and 0.17-0.24 Hz respectively. These values are higher than those reported for events located at Cerberus Fossae, indicating a higher stress drop for S1222a. Given that the event is located outside the Cerberus Fossae region, this might indicate that the source mechanism is different for events inside and outside Cerberus Fossae. Finally, this study demonstrated that contamination at higher frequencies needs to be taken into account when performing spectral analyses. EGF analyses might be the way to overcome such difficulty and understand better the dynamics of martian quakes.

8 Open Research

All raw waveform data are available through the InSight Mars SEIS Data Service @ IPGP, IRIS-DMC and NASA PDS (InSight Mars SEIS Data Service, 2019c). The event catalog is available from InSight Marsquake Service (InSight Marsquake Service, 2023).

Acknowledgments

We acknowledge NASA, CNES, partner agencies and institutions (UKSA, SSO, DLR, JPL, IPGP-CNRS, ETHZ, ICL, MPS-MPG), and the operators of JPL, SISMOC, MSDS, IRISDMC and PDS for providing SEED SEIS data. French co-authors acknowledge support of the French Space Agency CNES and Agence Nationale de la Recherche, ANR (ANR-19-CE31-0008-08). TK, ZX, WX, SM and PL acknowledge support of IdEx Université Paris Cité ANR-18-IDEX-0001. This research was carried out in part at the Jet Propulsion Laboratory, California Institute of Technology, under a contract with the National Aeronautics and Space Administration (80NM0018D0004). This paper is InSight Contribution Number 295.

References

- Abercrombie, R. E. (1995). Earthquake source scaling relationships from 1 to 5 ml using seismograms recorded at 2.5-km depth. *Journal of Geophysical Research: Solid Earth*, 100(B12), 24015-24036. Retrieved from <https://agupubs.onlinelibrary.wiley.com/doi/abs/10.1029/95JB02397>

- doi: <https://doi.org/10.1029/95JB02397>
- Aki, K., & Richards, P. (2002). Quantitative seismology, 2nd edition, chapter 10. *University Scientific Books, Sausalito, California*, 491-536.
- Allmann, B., & Shearer, P. (2009). Global variations of stress drop for moderate to large earthquakes. *Journal of Geophysical Research*, *114*(B1), B01310. doi: 10.1029/2008JB005821
- Banerdt, W. B., Smrekar, S. E., Banfield, D., Giardini, D., Golombek, M., Johnson, C. L., ... Wieczorek, M. (2020). Initial results from the InSight mission on Mars. *Nat. Geosci.*, *13*(3), 183–189. doi: 10.1038/s41561-020-0544-y
- Banfield, D., Rodriguez-Manfredi, J. A., Russell, C. T., Rowe, K. M., Leneman, D., Lai, H. R., ... Banerdt, W. B. (2019). InSight Auxiliary Payload Sensor Suite (APSS). *Space Sci. Rev.*, *215*(1), 4. doi: 10.1007/s11214-018-0570-x
- Boatwright, J. (1980, 02). A spectral theory for circular seismic sources; simple estimates of source dimension, dynamic stress drop, and radiated seismic energy. *Bulletin of the Seismological Society of America*, *70*(1), 1-27. Retrieved from <https://doi.org/10.1785/BSSA0700010001> doi: 10.1785/BSSA0700010001
- Brinkman, N., Stähler, S. C., Giardini, D., Schmelzbach, C., Khan, A., Jacob, A., ... Banerdt, W. B. (2021). First focal mechanisms of marsquakes. *J. Geophys. Res.: Planets*, *126*(4), e2020JE006546. doi: <https://doi.org/10.1029/2020JE006546>
- Broquet, A., & Andrews-Hanna, J. C. (2023, Feb 01). Geophysical evidence for an active mantle plume underneath elysium planitia on mars. *Nature Astronomy*, *7*(2), 160-169. Retrieved from <https://doi.org/10.1038/s41550-022-01836-3> doi: 10.1038/s41550-022-01836-3
- Brune, J. N. (1970). Tectonic stress and the spectra of seismic shear waves from earthquakes. *Journal of Geophysical Research (1896-1977)*, *75*(26), 4997-5009. Retrieved from <https://agupubs.onlinelibrary.wiley.com/doi/abs/10.1029/JB075i026p04997> doi: <https://doi.org/10.1029/JB075i026p04997>
- Carrasco, S., Knapmeyer-Endrun, B., Margerin, L., Schmelzbach, C., Onodera, K., Pan, L., ... others (2023). Empirical h/v spectral ratios at the insight landing site and implications for the martian subsurface structure. *Geophysical Journal International*, *232*(2), 1293–1310.
- Ceylan, S., Clinton, J. F., Giardini, D., Böse, M., Charalambous, C., van Driel, M., ... Perrin, C. (2021). Companion guide to the marsquake catalog from InSight, Sols 0–478: Data content and non-seismic events. *Phys. Earth Planet. Inter.*, *310*, 106597. doi: <https://doi.org/10.1016/j.pepi.2020.106597>
- Clinton, J. F., Ceylan, S., van Driel, M., Giardini, D., Stähler, S. C., Böse, M., ... Stott, A. E. (2021). The marsquake catalogue from insight, sols 0–478. *Phys. Earth Planet. Inter.*, *310*, 106595. doi: <https://doi.org/10.1016/j.pepi.2020.106595>
- Clinton, J. F., Giardini, D., Böse, M., Ceylan, S., van Driel, M., Euchner, F., ... Teanby, N. A. (2018). The Marsquake Service: Securing Daily Analysis of SEIS Data and Building the Martian Seismicity Catalogue for InSight. *Space Sci. Rev.*, *214*, 133. doi: 10.1007/s11214-018-0567-5
- Dahmen, N. L., Zenhäusern, G., Clinton, J. F., Giardini, D., Stähler, S. C., Ceylan, S., ... Banerdt, W. B. (2021, 10). Resonances and Lander Modes Observed by InSight on Mars (1–9 Hz). *Bull. Seismol. Soc. Am.*, *111*(6), 2924-2950. doi: 10.1785/0120210056
- Drilleau, M., Samuel, H., Garcia, R. F., Rivoldini, A., Perrin, C., Michaut, C., ... Banerdt, W. B. (2022). Marsquake locations and 1-d seismic models for mars from insight data. *Journal of Geophysical Research: Planets*, *127*(9), e2021JE007067. Retrieved from <https://agupubs.onlinelibrary.wiley.com/doi/abs/10.1029/2021JE007067> (e2021JE007067 2021JE007067) doi: <https://doi.org/10.1029/2021JE007067>
- Durán, C., Khan, A., Ceylan, S., Zenhäusern, G., Stähler, S., Clinton, J., & Gi-

- ardini, D. (2022). Seismology on mars: An analysis of direct, reflected, and converted seismic body waves with implications for interior structure. *Phys. Earth Planet. Inter.*, 325, 106851. doi: <https://doi.org/10.1016/j.pepi.2022.106851>
- Eulenfeld, T., Dahm, T., Heimann, S., & Wegler, U. (2021, 11). Fast and Robust Earthquake Source Spectra and Moment Magnitudes from Envelope Inversion. *Bulletin of the Seismological Society of America*, 112(2), 878-893. Retrieved from <https://doi.org/10.1785/0120210200> doi: 10.1785/0120210200
- Eulenfeld, T., & Wegler, U. (2016, 03). Measurement of intrinsic and scattering attenuation of shear waves in two sedimentary basins and comparison to crystalline sites in Germany. *Geophysical Journal International*, 205(2), 744-757. Retrieved from <https://doi.org/10.1093/gji/ggw035> doi: 10.1093/gji/ggw035
- Fayon, L., Knapmeyer-Endrun, B., Lognonné, P., Bierwirth, M., Kramer, A., Delage, P., ... Banerdt, W. B. (2018). A numerical model of the seismology system transfer matrix and resonances: Application to seismic rotational seismology and dynamic ground interaction. *Space Science Reviews*, 214(8), 119. Retrieved from <https://doi.org/10.1007/s11214-018-0555-9> doi: 10.1007/s11214-018-0555-9
- Garcia, R. F., Daubar, I. J., Beucler, É., Posiolova, L. V., Collins, G. S., Lognonné, P., ... Banerdt, W. B. (2022, Sep 19). Newly formed craters on mars located using seismic and acoustic wave data from insight. *Nature Geoscience*. Retrieved from <https://doi.org/10.1038/s41561-022-01014-0> doi: 10.1038/s41561-022-01014-0
- Giardini, D., Lognonné, P., Banerdt, W. B., Pike, W. T., Christensen, U., Ceylan, S., ... Yana, C. (2020). The Seismicity of Mars. *Nat. Geosci.* doi: 10.1038/s41561-020-0539-8
- Hartzell, S. H. (1978). Earthquake aftershocks as green's functions. *Geophysical Research Letters*, 5(1), 1-4. Retrieved from <https://agupubs.onlinelibrary.wiley.com/doi/abs/10.1029/GL005i001p00001> doi: <https://doi.org/10.1029/GL005i001p00001>
- Hobiger, M., Hallo, M., Schmelzbach, C., Stähler, S. C., Fäh, D., Giardini, D., ... Banerdt, W. B. (2021, Nov 23). The shallow structure of mars at the insight landing site from inversion of ambient vibrations. *Nature Communications*, 12(1), 6756. doi: 10.1038/s41467-021-26957-7
- InSight Mars SEIS Data Service. (2019a). *aSEIS raw data, Insight Mission. IPGP, JPL, CNES, ETHZ, ICL, MPS, ISAE-Supaero, LPG, MFSC.* doi: {10.18715/SEIS.INSIGHT.XB\2016}
- InSight Mars SEIS Data Service. (2019b). *bInSight SEIS Data Bundle. PDS Geosciences (GEO) Node.* doi: {10.17189/1517570}
- InSight Mars SEIS Data Service. (2019c). *Seis raw data, insight mission. IPGP, JPL, CNES, ETHZ, ICL, MPS, ISAE-Supaero, LPG, MFSC.* Retrieved from https://datacenter.ipgp.fr/networks/detail/XB_2016/ doi: 10.18715/SEIS.INSIGHT.XB_2016
- InSight Marsquake Service. (2023). *Mars seismic catalogue, insight mission; v13 2023-01-01.* ETHZ, IPGP, JPL, ICL, Univ. Bristol. Retrieved from <https://www.insight.ethz.ch/seismicity/catalog/v13> doi: 10.12686/a19
- Jacob, A., Plasman, M., Perrin, C., Fuji, N., Lognonné, P., Xu, Z., ... Banerdt, W. (2022). Seismic sources of insight marsquakes and seismotectonic context of elysium planitia, mars. *Tectonophysics*, 837, 229434. Retrieved from <https://www.sciencedirect.com/science/article/pii/S0040195122002281> doi: <https://doi.org/10.1016/j.tecto.2022.229434>
- Kaneko, Y., & Shearer, P. (2014). Seismic source spectra and estimated stress drop derived from cohesive-zone models of circular subshear rupture. *Geophysical Journal International*, 197(2), 1002-1015.
- Kawamura, T., Clinton, J. F., Zenhäusern, G., Ceylan, S., Horleston, A. C., Dah-

- men, N. L., ... Banerdt, W. B. (2022). S1222a - the largest marsquake detected by insight. *Geophysical Research Letters*, 49, e2022GL101543. Retrieved from <https://agupubs.onlinelibrary.wiley.com/doi/abs/10.1029/2022GL101543> (e2022GL101543 2022GL101543) doi: <https://doi.org/10.1029/2022GL101543>
- Kawamura, T., Lognonné, P., Nishikawa, Y., & Tanaka, S. (2017). Evaluation of deep moonquake source parameters: Implication for fault characteristics and thermal state. *Journal of Geophysical Research: Planets*, 122, 1487-1504. doi: 10.1002/2016JE005147
- Kenda, B., Drilleau, M., Garcia, R. F., Kawamura, T., Murdoch, N., Compaire, N., ... Spohn, T. (2020). Subsurface structure at the insight landing site from compliance measurements by seismic and meteorological experiments. *J. Geophys. Res.: Planets*, 125(6), e2020JE006387. doi: <https://doi.org/10.1029/2020JE006387>
- Khan, A., Ceylan, S., van Driel, M., Giardini, D., Lognonné, P., Samuel, H., ... Banerdt, W. B. (2021). Upper mantle structure of Mars from InSight seismic data. *Science*, 373(6553), 434-438. doi: 10.1126/science.abf2966
- Knapmeyer-Endrun, B., Panning, M. P., Bissig, F., Joshi, R., Khan, A., Kim, D., ... Banerdt, W. B. (2021). Thickness and structure of the martian crust from insight seismic data. *Science*, 373(6553), 438-443. doi: 10.1126/science.abf8966
- Lognonné, P., Banerdt, W., Giardini, D., Pike, W., Christensen, U., Laudet, P., ... Wookey, J. (2019). SEIS: Insight's Seismic Experiment for Internal Structure of Mars. *Space Sci. Rev.*, 215(1), 12. doi: 10.1007/s11214-018-0574-6
- Lognonné, P., Banerdt, W., Pike, W., Giardini, D., Christensen, U., Garcia, R., ... Zweifel, P. (2020). Constraints on the shallow elastic and anelastic structure of Mars from InSight seismic data. *Nat. Geosci.* doi: 10.1038/s41561-020-0536-y
- Madariaga, R. (1976). Dynamics of an expanding circular fault. *Bulletin of the Seismological Society of America*, 66(3), 639-666. doi: 10.1785/BSSA0660030639
- Posiolova, L. V., Lognonné, P., Banerdt, W. B., Clinton, J., Collins, G. S., Kawamura, T., ... Zenhäusern, G. (2022). Largest recent impact craters on mars: Orbital imaging and surface seismic co-investigation. *Science*, 378(6618), 412-417. Retrieved from <https://www.science.org/doi/abs/10.1126/science.abq7704> doi: 10.1126/science.abq7704
- Prieto, G. A., Shearer, P. M., Vernon, F. L., & Kilb, D. (2004). Earthquake source scaling and self-similarity estimation from stacking p and s spectra. *Journal of Geophysical Research: Solid Earth*, 109(B8). Retrieved from <https://agupubs.onlinelibrary.wiley.com/doi/abs/10.1029/2004JB003084> doi: <https://doi.org/10.1029/2004JB003084>
- Sato, T., & Hirasawa, T. (1973). Body wave spectra from propagating shear cracks. *Journal of Physics of the Earth*, 21(4), 415-431. doi: 10.4294/jpe1952.21.415
- Shearer, P. M. (2019). *Introduction to seismology* (3rd ed.). Cambridge University Press. doi: 10.1017/9781316877111
- Shearer, P. M., Prieto, G. A., & Hauksson, E. (2006). Comprehensive analysis of earthquake source spectra in southern california. *Journal of Geophysical Research: Solid Earth*, 111(B6). Retrieved from <https://agupubs.onlinelibrary.wiley.com/doi/abs/10.1029/2005JB003979> doi: <https://doi.org/10.1029/2005JB003979>
- Shi, J., Plasman, M., Knapmeyer-Endrun, B., Xu, Z., Kawamura, T., Lognonné, P., ... Wang, T. (2023). High-frequency receiver functions with event s1222a reveal a discontinuity in the martian shallow crust. *Geophysical Research Letters*, 50(5), e2022GL101627. Retrieved from <https://agupubs.onlinelibrary.wiley.com/doi/abs/10.1029/2022GL101627> (e2022GL101627 2022GL101627) doi: <https://doi.org/10.1029/2022GL101627>
- Stähler, S. C., Khan, A., Banerdt, W. B., Lognonné, P., Giardini, D., Ceylan, S., ... Smrekar, S. E. (2021). Seismic detection of the martian core. *Science*, 373(6553), 443-448. doi: 10.1126/science.abi7730

- Stähler, S. C., Mittelholz, A., Perrin, C., Kawamura, T., Kim, D., Knapmeyer, M., ... Banerdt, W. B. (2022, Oct 27). Tectonics of cerberus fossae unveiled by marsquakes. *Nature Astronomy*. Retrieved from <https://doi.org/10.1038/s41550-022-01803-y> doi: 10.1038/s41550-022-01803-y
- Towhata, I. (2008). Geotechnical earthquake engineering, chapter 6. *Springer Berlin, Heidelberg*, 88-120. doi: 10.1007/978-3-540-35783-4
- Uchide, T., & Imanishi, K. (2016). Small earthquakes deviate from the omega-square model as revealed by multiple spectral ratio analysis. *Bulletin of the Seismological Society of America*, 106, 1357-1363.
- Xiao, W., Kawamura, T., Xu, Z., Carrasco, S., Onodera, K., Sainton, G., ... Banerdt, W. B. (2023). Evaluation of s1222a source parameters based on site effect simulation and implication for the event origin. *Geophysical Research Letters*.

Figure3.

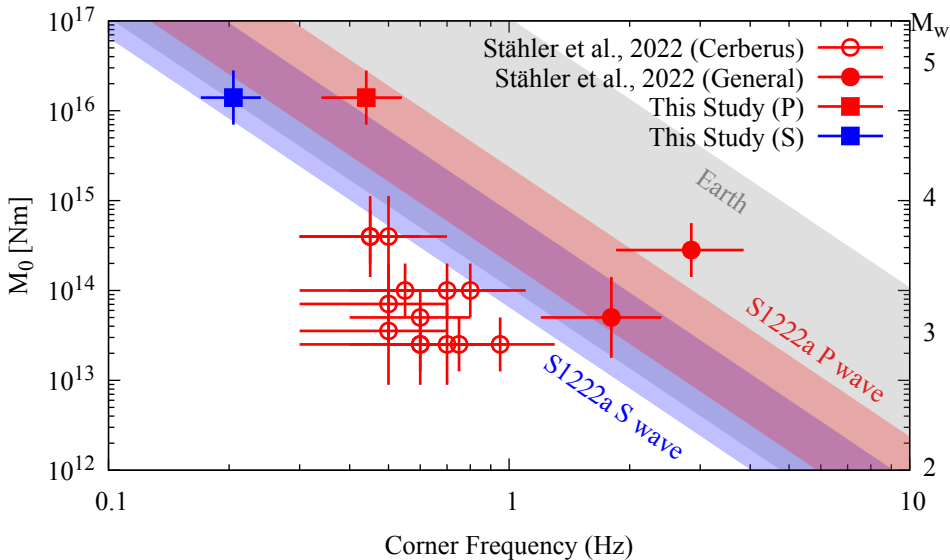


Figure2.

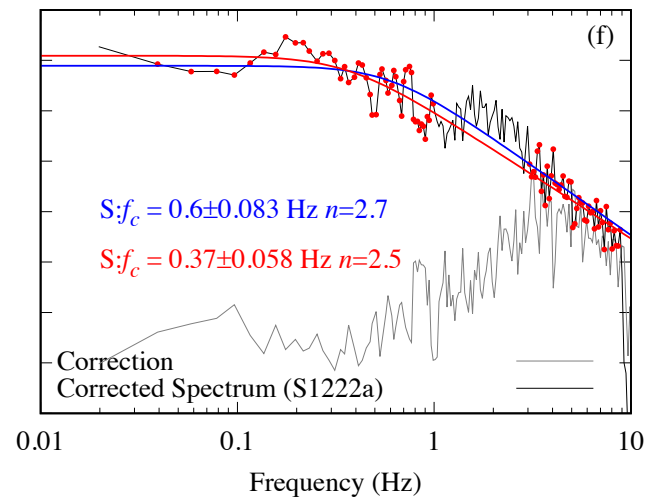
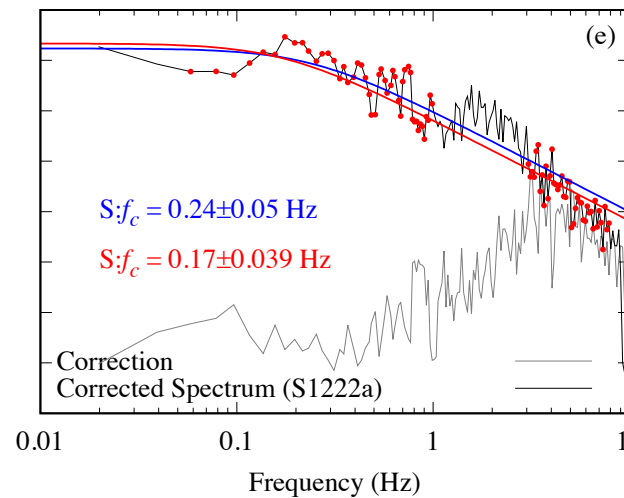
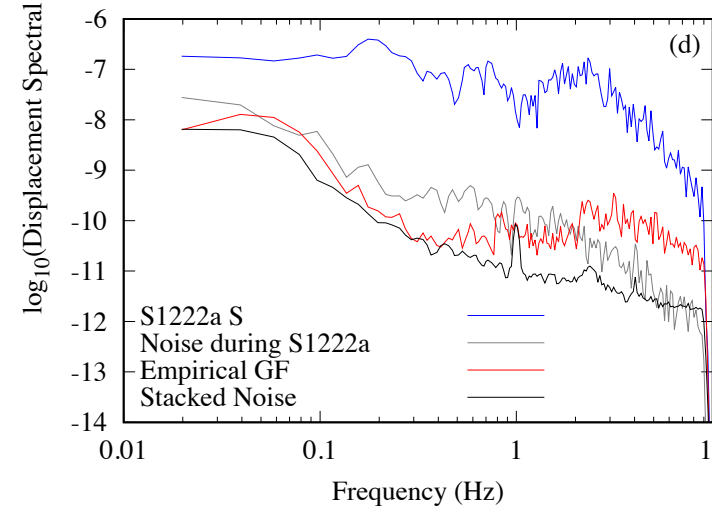
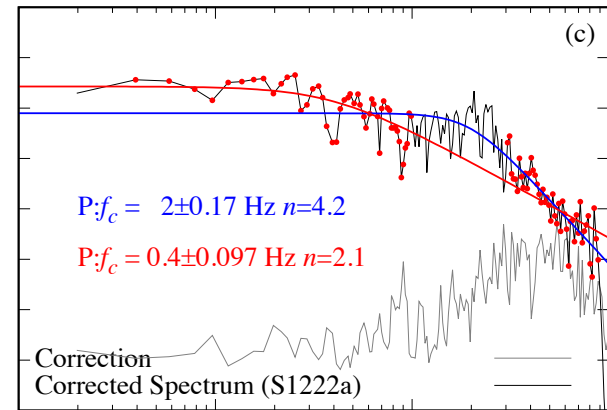
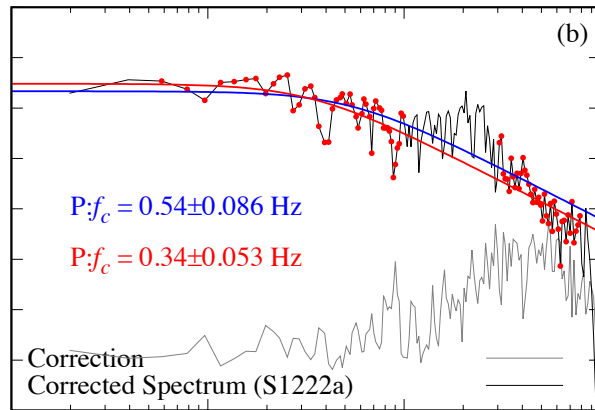
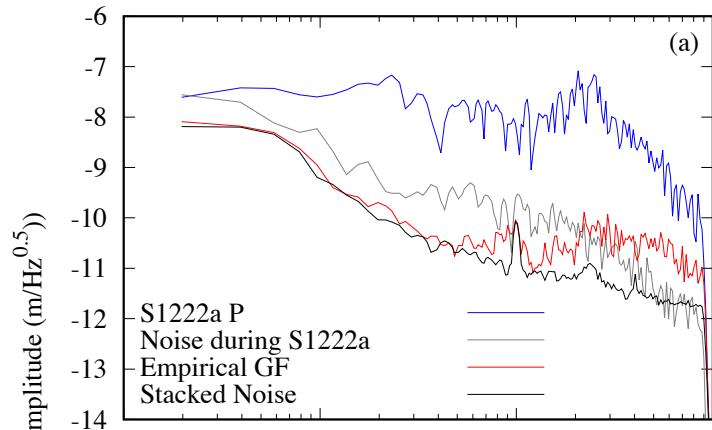
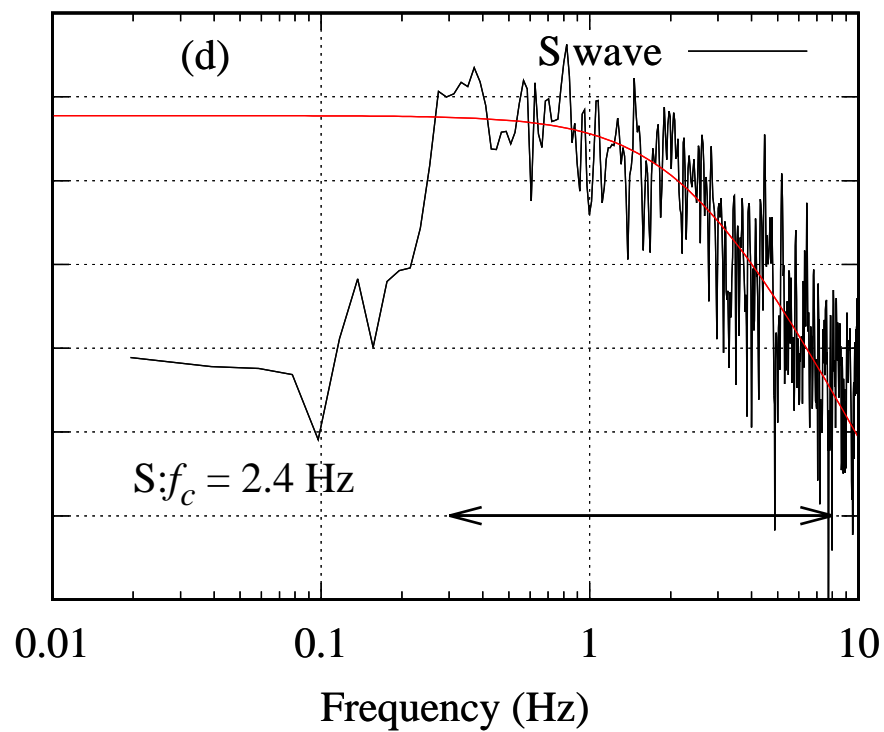
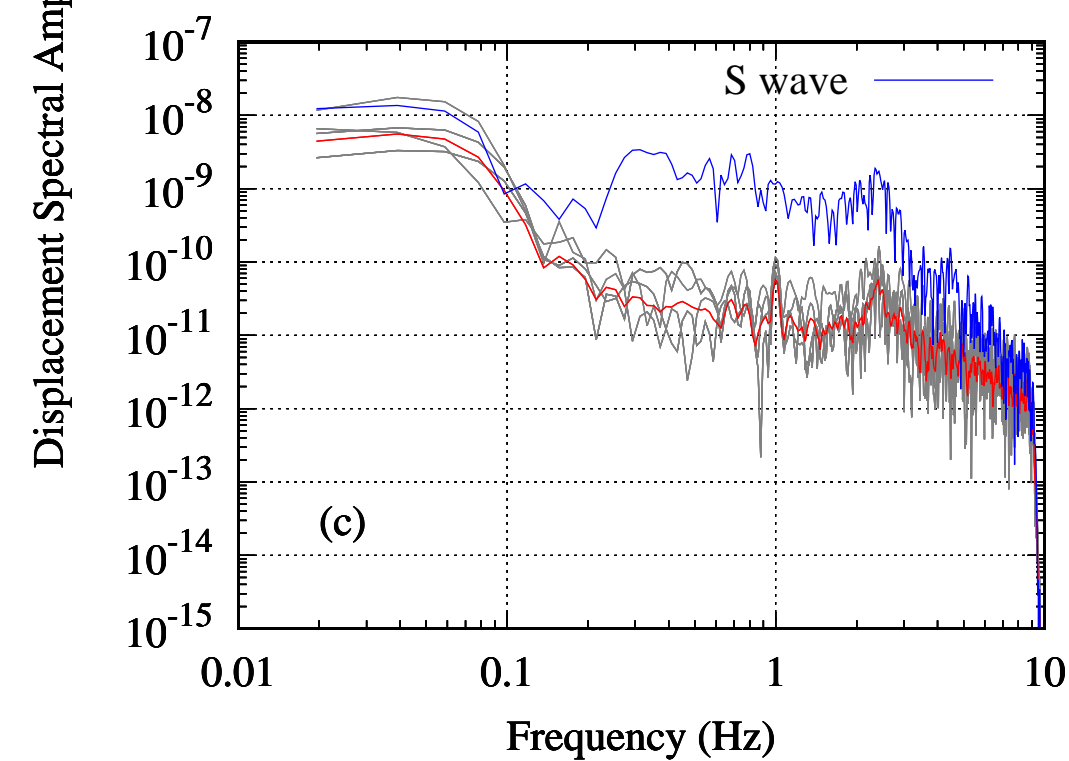
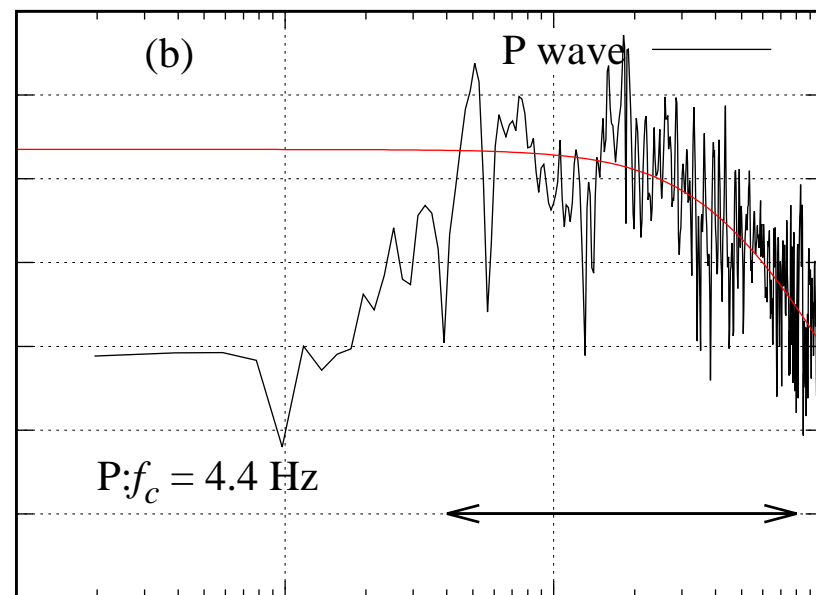
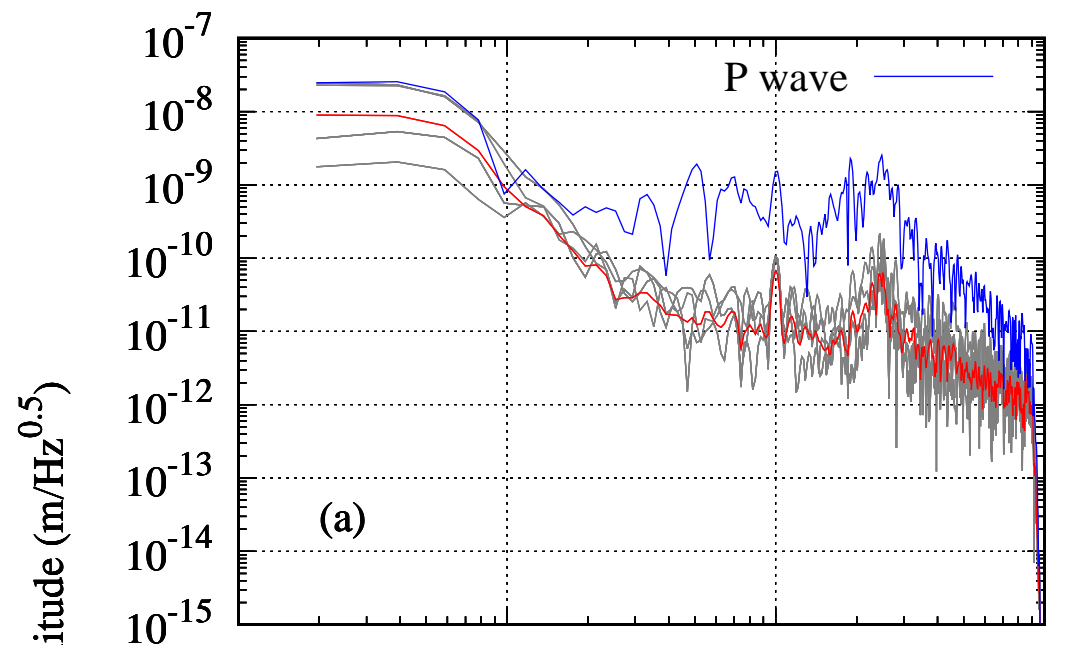


Figure1.



Supporting Information for ”Source Parameters of S1222a Marsquake obtained from Spectral Analyses using Empirical Green’s Function”

Taichi Kawamura¹, Zongbo Xu¹, Wanbo Xiao¹, Ludovic Margerin², Sabrina

Menina¹, Philippe Lognonné¹, William Bruce Banerdt³

¹Université Paris Cité, Institut de physique du globe de Paris, CNRS, Paris, France

²Institut de Recherche en Astrophysique et Planétologie, Toulouse, France

³Jet Propulsion Laboratory, California Institute of Technology, CA, USA

Contents of this file

1. Tables S1 to S2
2. Figures S1 to S11

Table S1. Events used for EGF analyses of S1094b^a

Event Name	Event Type	Event Quality	Magnitude	ts-tp (s)
S1094	VF	A	4.0	342
S0218a	VF	B	2.5	336
S0387a	VF	B	2.1	347
S0424c	VF	B	2.2	338
S0869b	VF	B	2.5	330

^a The first event of the table is the reference event.

Table S2. Events used for EGF analyses of S1222a^b

Event Name	Event Type	Event Quality	Magnitude	ts-tp (s)
S1222a	BB	A	4.7	214
S1135c	HF	B	1.8	216
S1091a	HF	B	1.8	218
S1082c	HF	B	2.3	229
S1040b	HF	B	2.1	218
S1024c	HF	B	2.0	235
S0997a	HF	B	2.1	232
S0882a	VF	B	2.4	234
S0758a	HF	B	2.1	190
S0756a	VF	B	2.8	206
S0436c	HF	B	2.1	232
S0334a	VF	B	2.1	214
S0327c	HF	B	1.9	199
S0228c	HF	B	1.9	232
S0183a	LF	B	2.7	194

^b The first event of the table is the reference event.

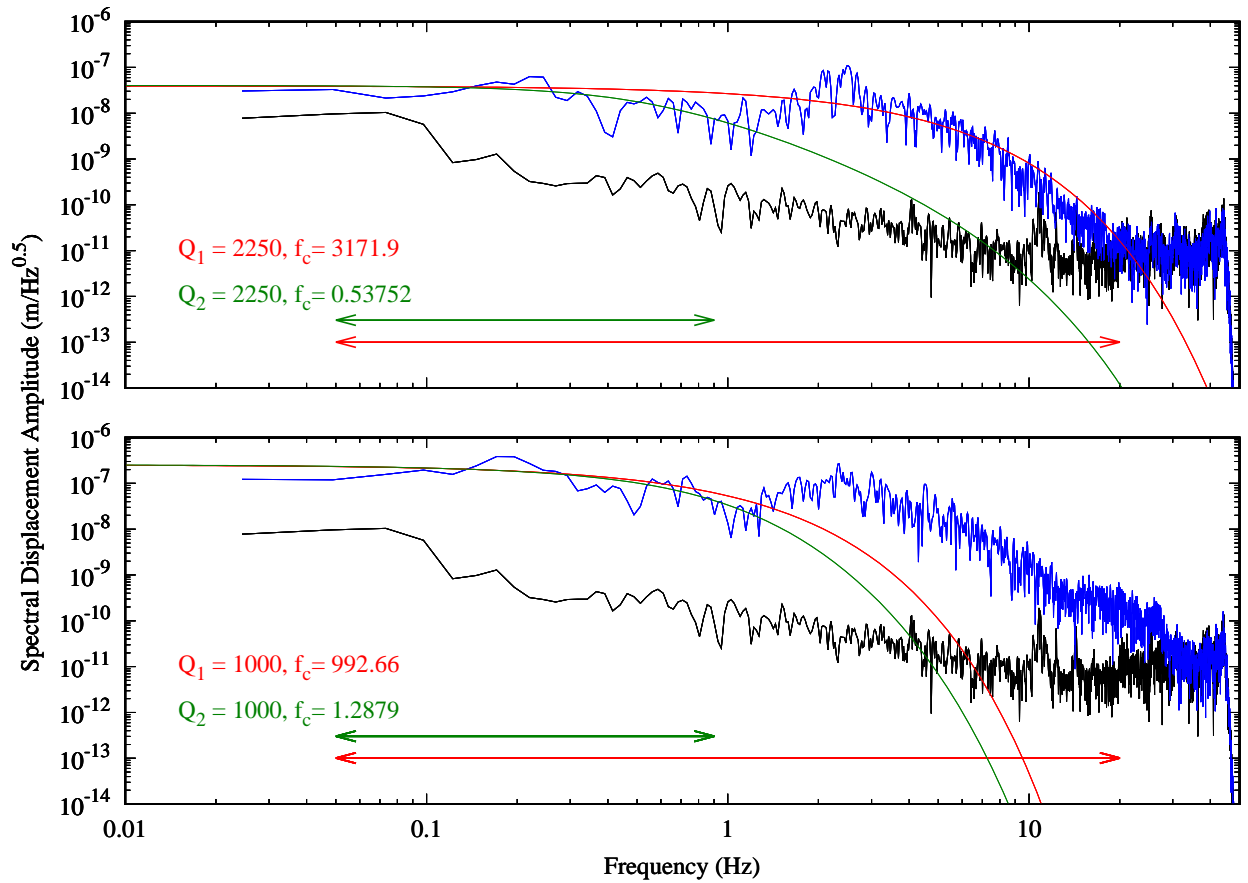


Figure S1. S1222a spectra for P and S waves. The top panel shows the P spectrum and the bottom panel shows the S spectrum. The seismic spectra are shown in blue and the noise spectra is shown in black. The red line is the fitting with Eq. ?? using reference Q values from (?, ?) and wide frequency band (0.05-20Hz; shown in red arrow)). The green line shows the result of the fitting with the narrow frequency band (0.05-0.9Hz; shown in green arrow).

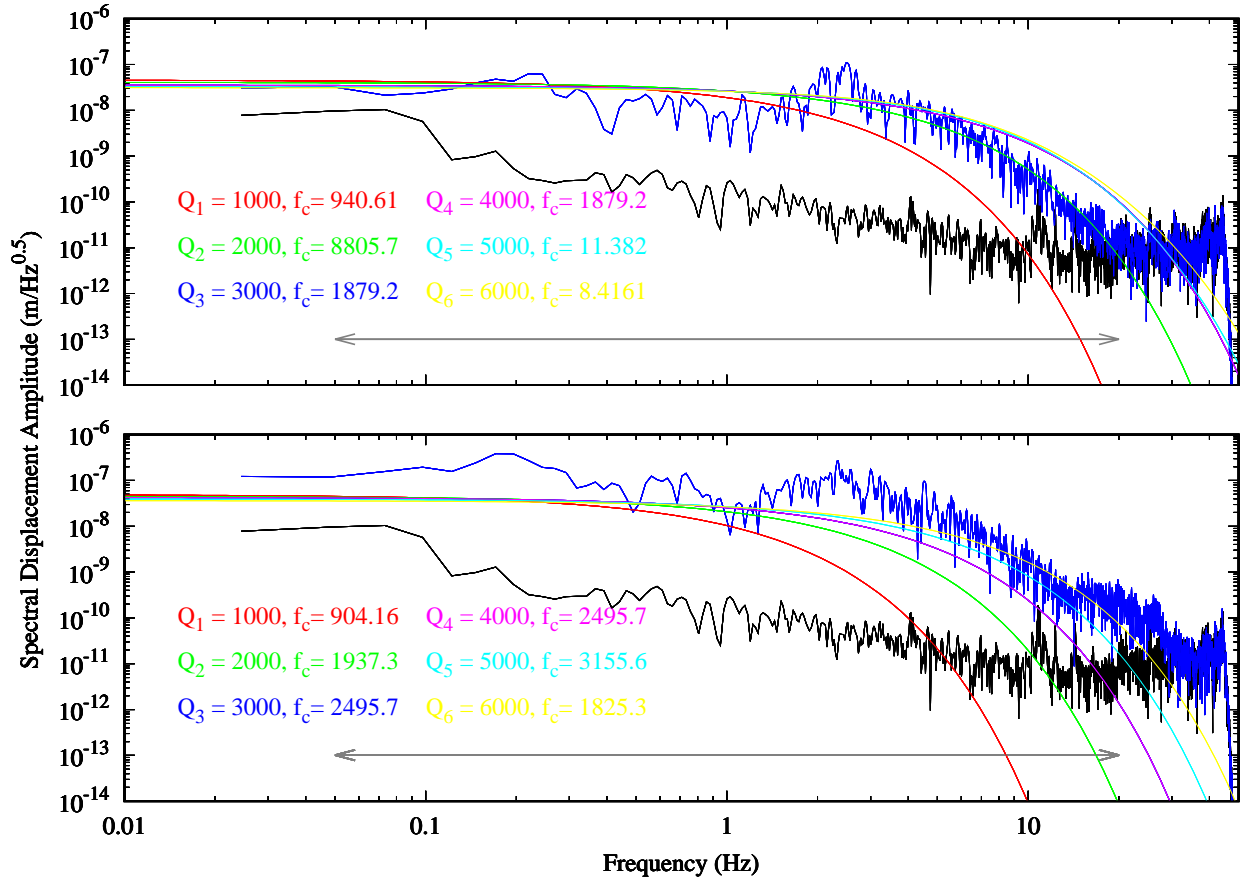


Figure S2. Results of Raw S1222a spectra fitted to ω^2 model with various Q factor. 0.05-20Hz was used to fit the model to the observation data. Even with the wide variety of Q that was used to explain the observations, we were not able to find a reasonable solution. For most of the cases, we found f_c extremely high and outside the frequency band we are using for the analyses. This implies that the decay of S1222a can be almost fully explained with attenuation, which is unreasonable following the former study which obtained f_c within the frequency band of the fit.

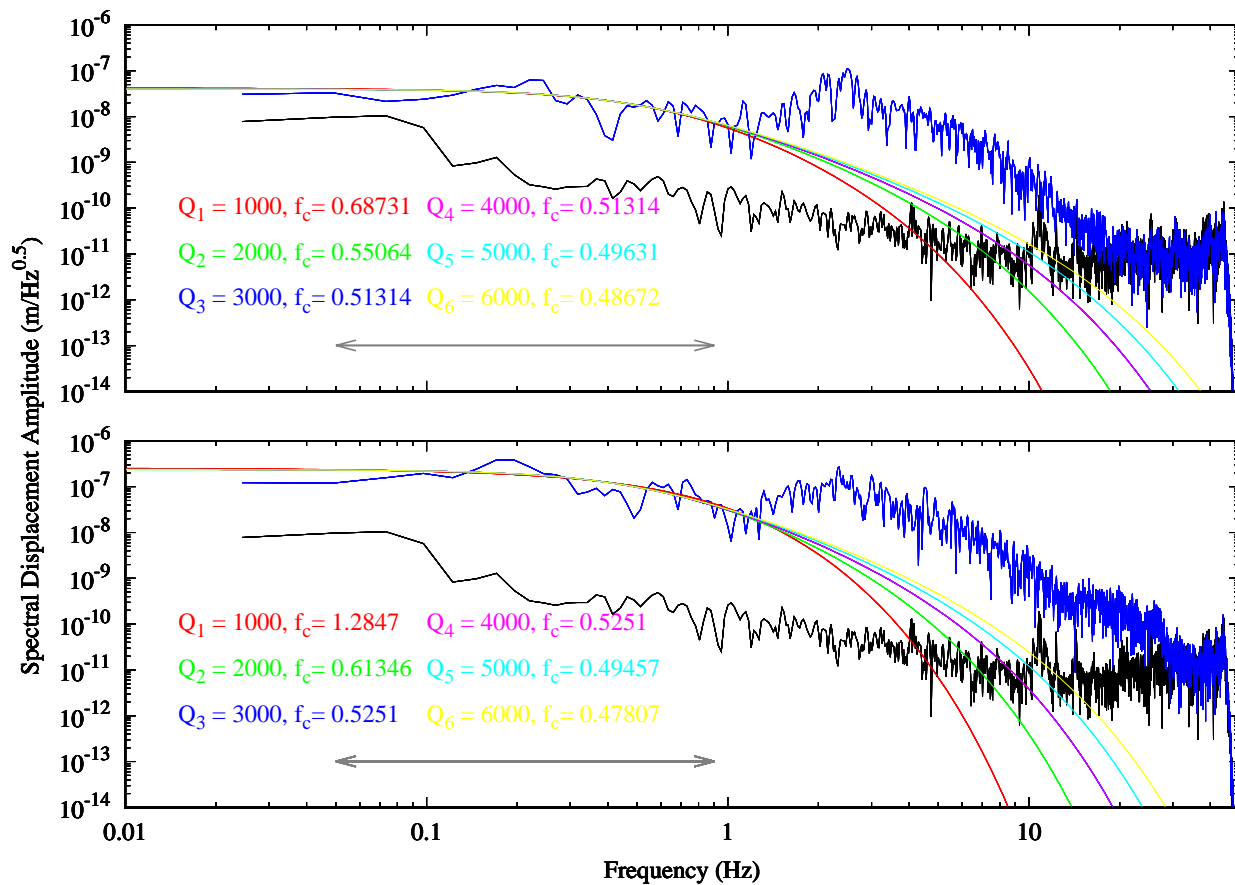


Figure S3. Results of Raw S1222a spectra fitted to ω^2 model with various Q factor. 0.05-8Hz was used to fit the model to the observation data. The obtained reasonable f_c for wide range of Q value. We found that the analyses suffer from the trade off between f_c and Q and since we excluded the high frequency portion of the spectra, we were not able to resolve the difference between different Q values.

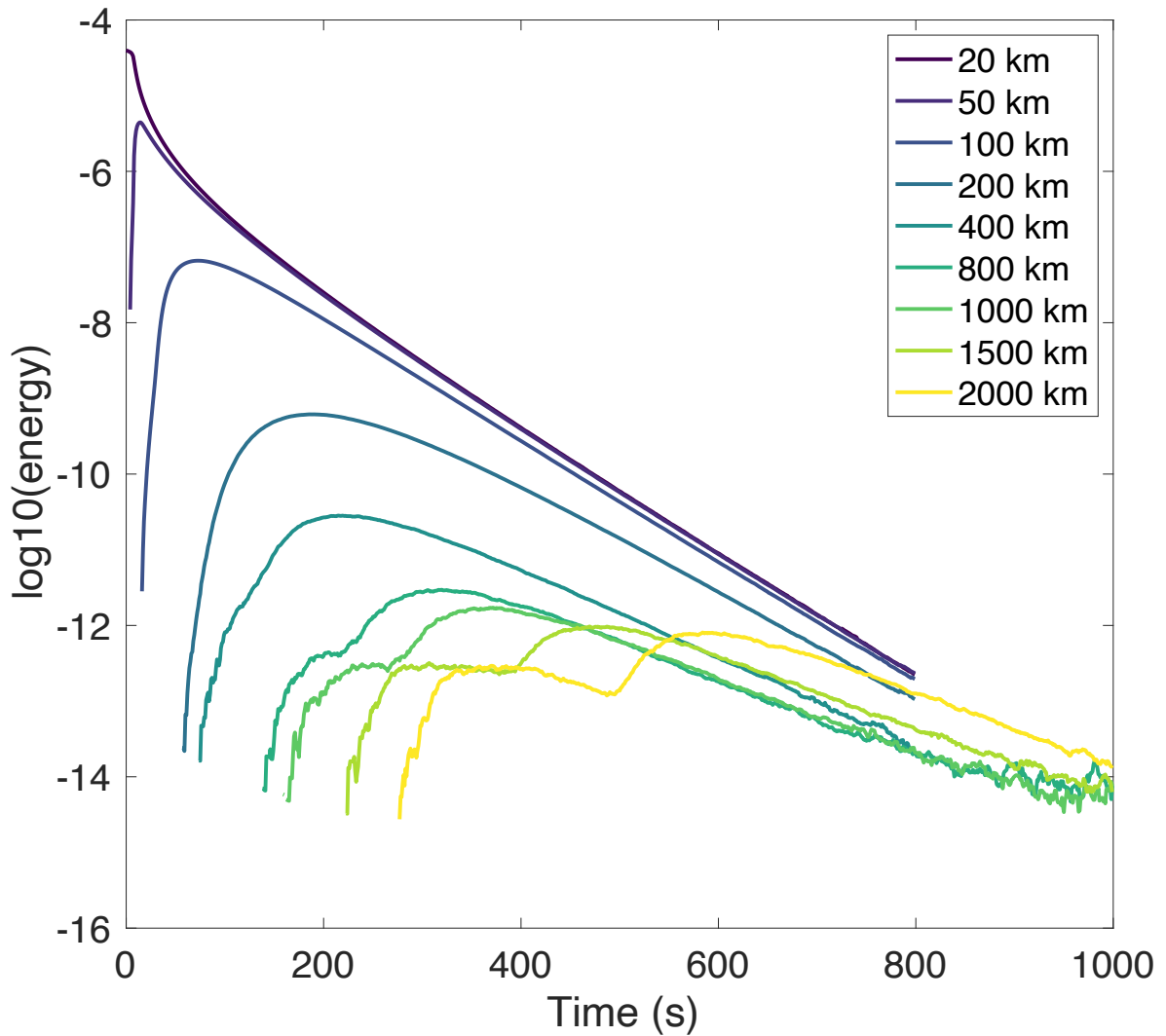


Figure S4. Synthetic coda evolution with diffusive subsurface structure. The calculation was made with 60km diffusive crust with $Q_{scattering} = 56$ and $Q_{\mu} = 2.35 \times 10^3$ overlying on a mantle with $Q_{scattering} = 2.35 \times 10^{21}$ and $Q_{\mu} = 2.35 \times 10^{21}$. The model was chosen so that it well reproduces the observed coda evolution for VF type events. While the envelope shape change drastically at short distances, it shows moderate change after 200km distance.

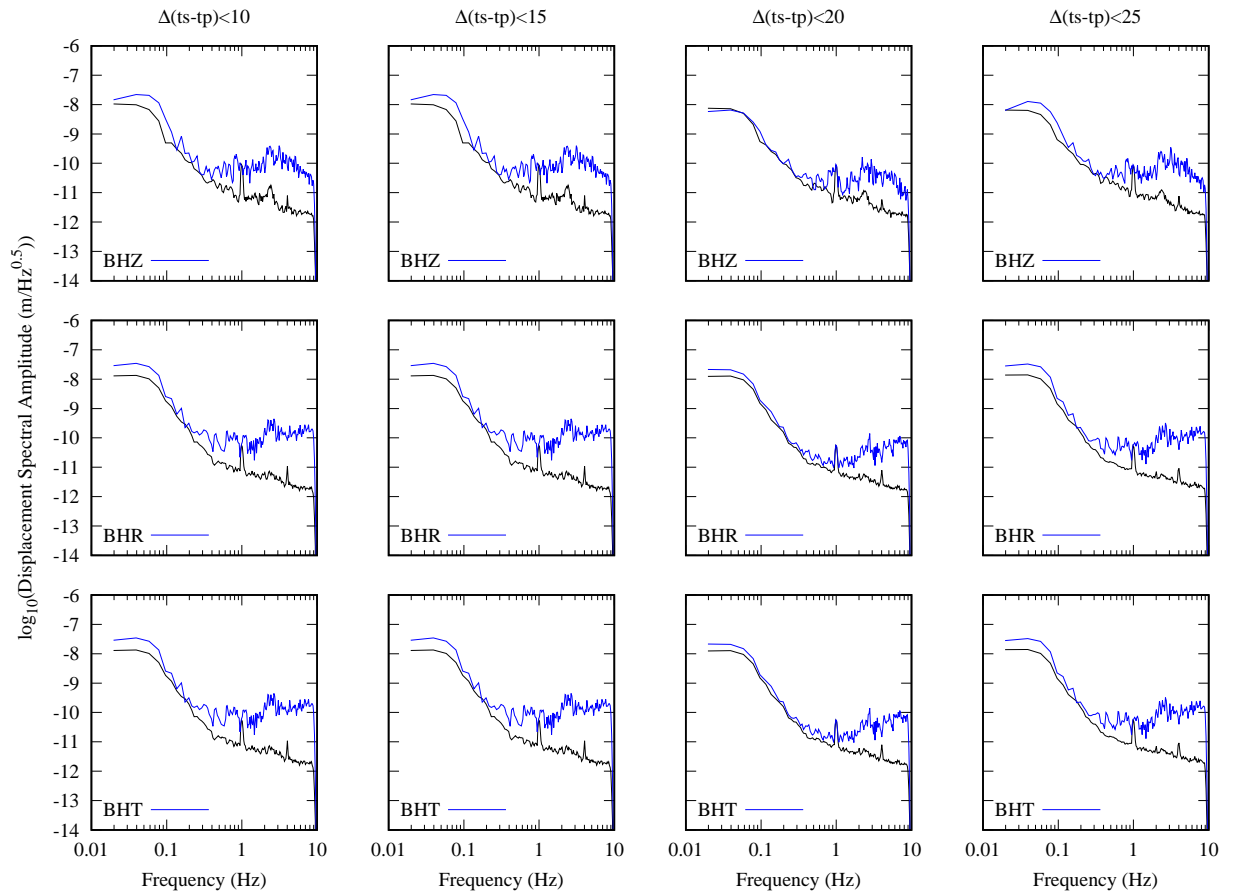


Figure S5. Comparison of EGFs calculated with different $ts-tp$ margin ($\Delta(ts-tp)$). $\Delta(ts-tp)$ is defined as the difference that we accept for $ts-tp$ time with respect to the reference value (i.e. S1222a: $ts-tp=214s$). Each column shows the different $\Delta(ts-tp)$ and each row shows the vertical, radial and transverse component. The blue lines show the EGFs and the black line is the stacked noise level. The difference is minor and we chose $\Delta(ts-tp) = 25s$ to have larger number of events.

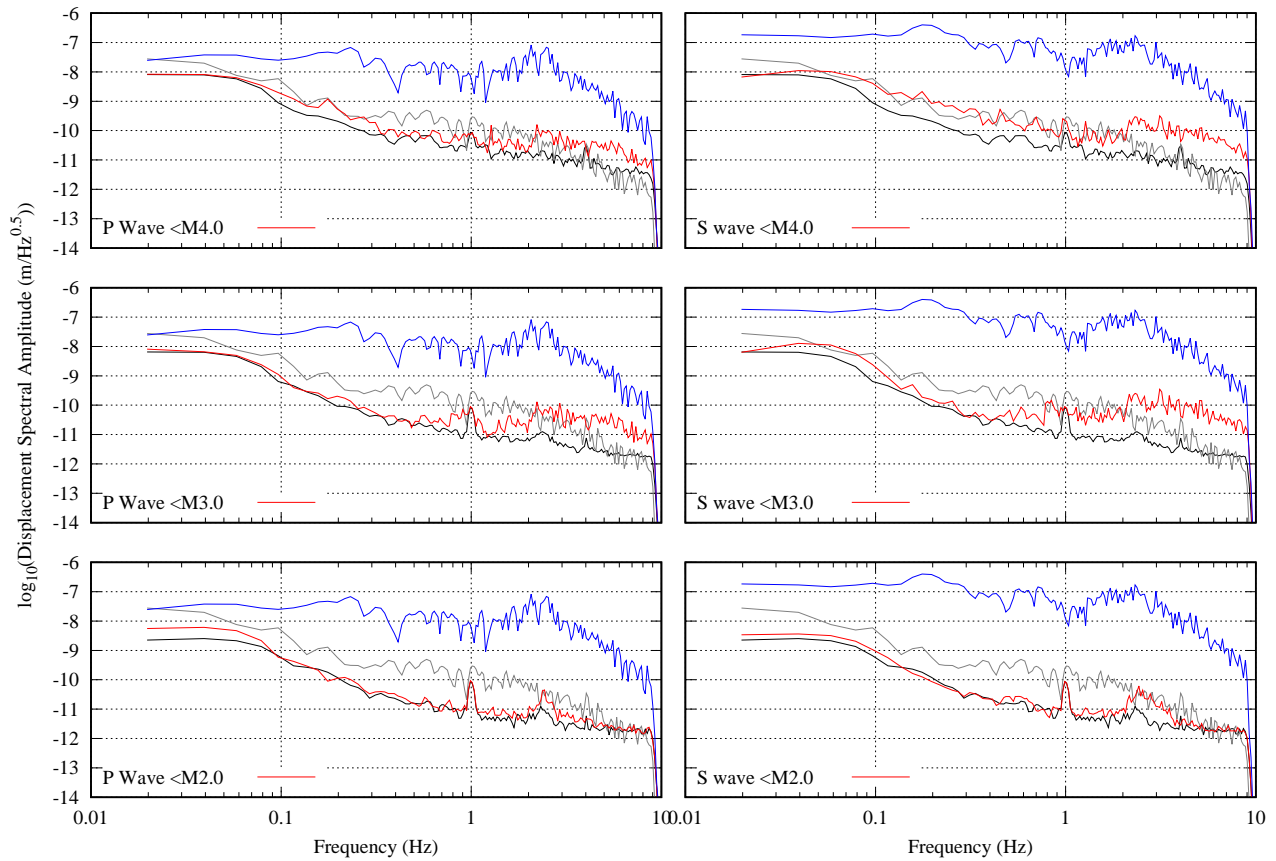


Figure S6. Comparison of EGFs calculated with different magnitude threshold. For each row we set the maximum magnitude to be included in the EGF estimation at $M=2.0$, 3.0 and 4.0 . The left and right column show the P and S wave respectively. The red lines are the EGFs obtained and the black lines are the stacked noise. The blue lines are the spectra of S1222a and the gray lines are the noise spectra at the time of S1222a events. We found that when we take $M=2.0$ as our threshold, the obtained EGFs have low S/N and they almost overlap with the noise except for the peak around 2.4Hz . On the other hand, for $M=3.0$ and 4.0 , we see the characteristic shape of the enhancement at the high frequency which well represents the contamination that we observed in the original data. Thus, we chose smaller value of $M=3.0$ as our threshold to have smaller impact of corner frequencies of these events to the EGFs.

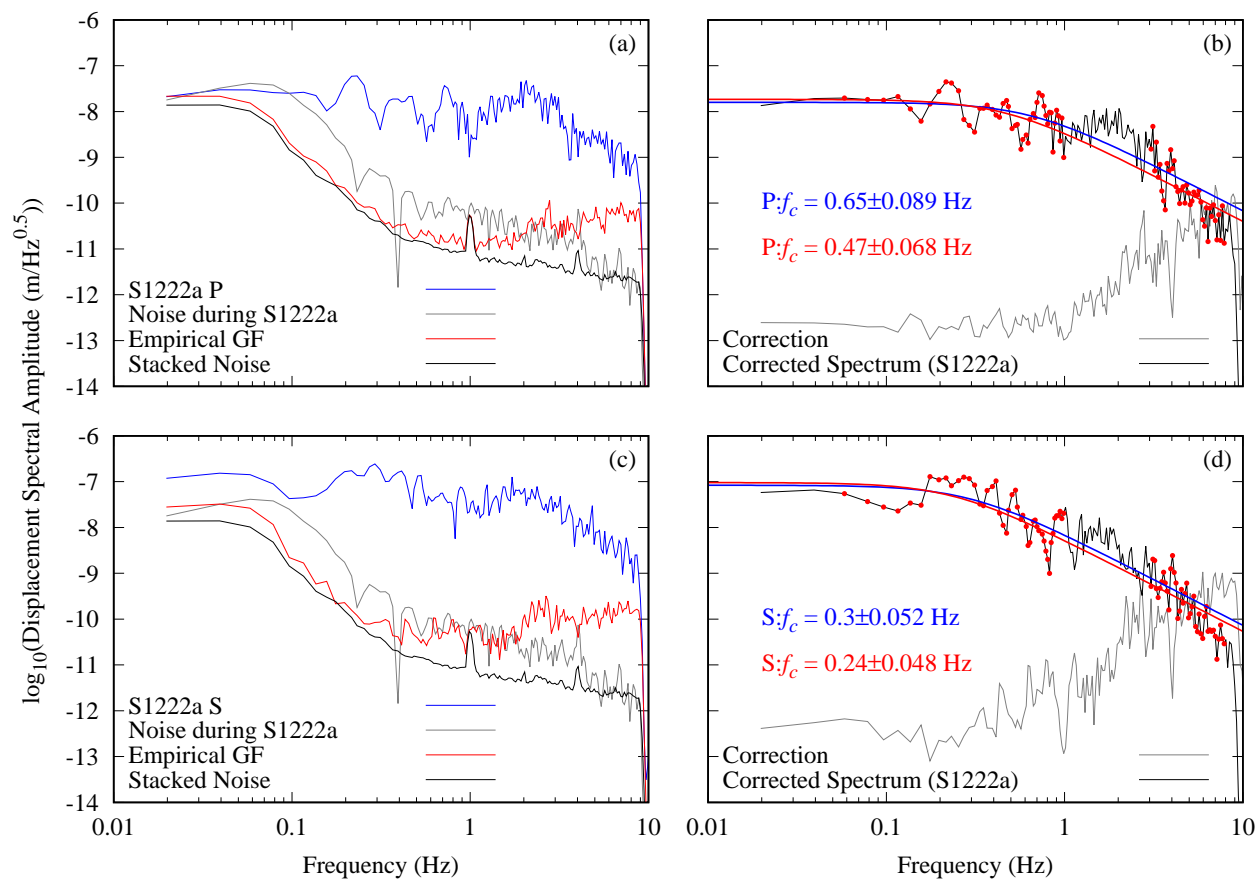


Figure S7. Empirical Green's Function (EGF) analyses performed for S1222a on the radial component. We used the same setting as Figure 3 in the main text. Note that since not all events have their back azimuth estimated from the data, we took both N and E component and stacked to obtain the EGF and the stacked noise

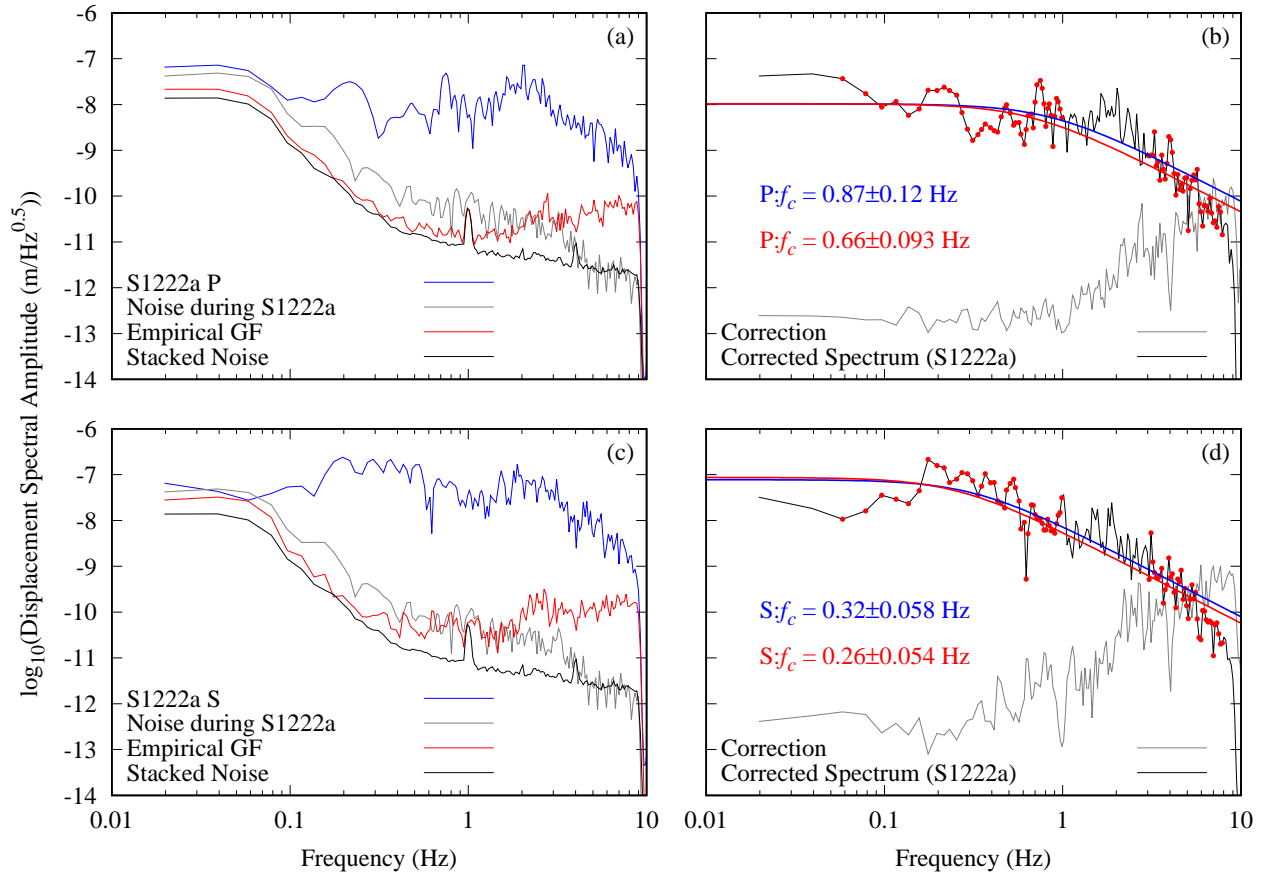


Figure S8. Empirical Green's Function (EGF) analyses performed for S1222a on the transverse component. We used the same setting as Figure 2 in the main text. Note that since not all events have their back azimuth estimated from the data, we took both N and E component and stacked to obtain the EGF and the stacked noise

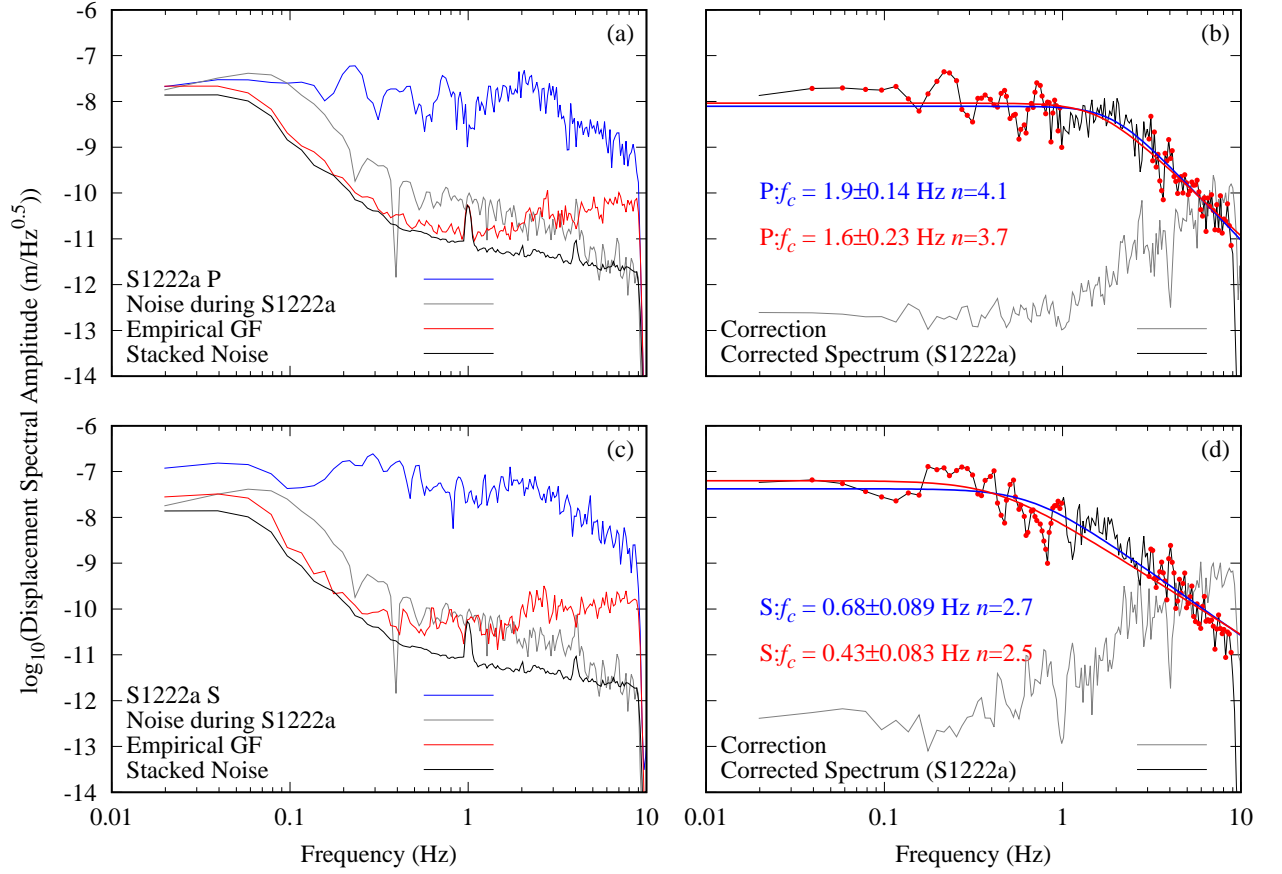


Figure S9. Empirical Green's Function (EGF) analyses performed for S1222a with general form of a source time function on radial component $\gamma = 1$. We used the same setting as Figure 2 in the main text. Note that since not all events have their back azimuth estimated from the data, we took both N and E component and stacked to obtain the EGF and the stacked noise.

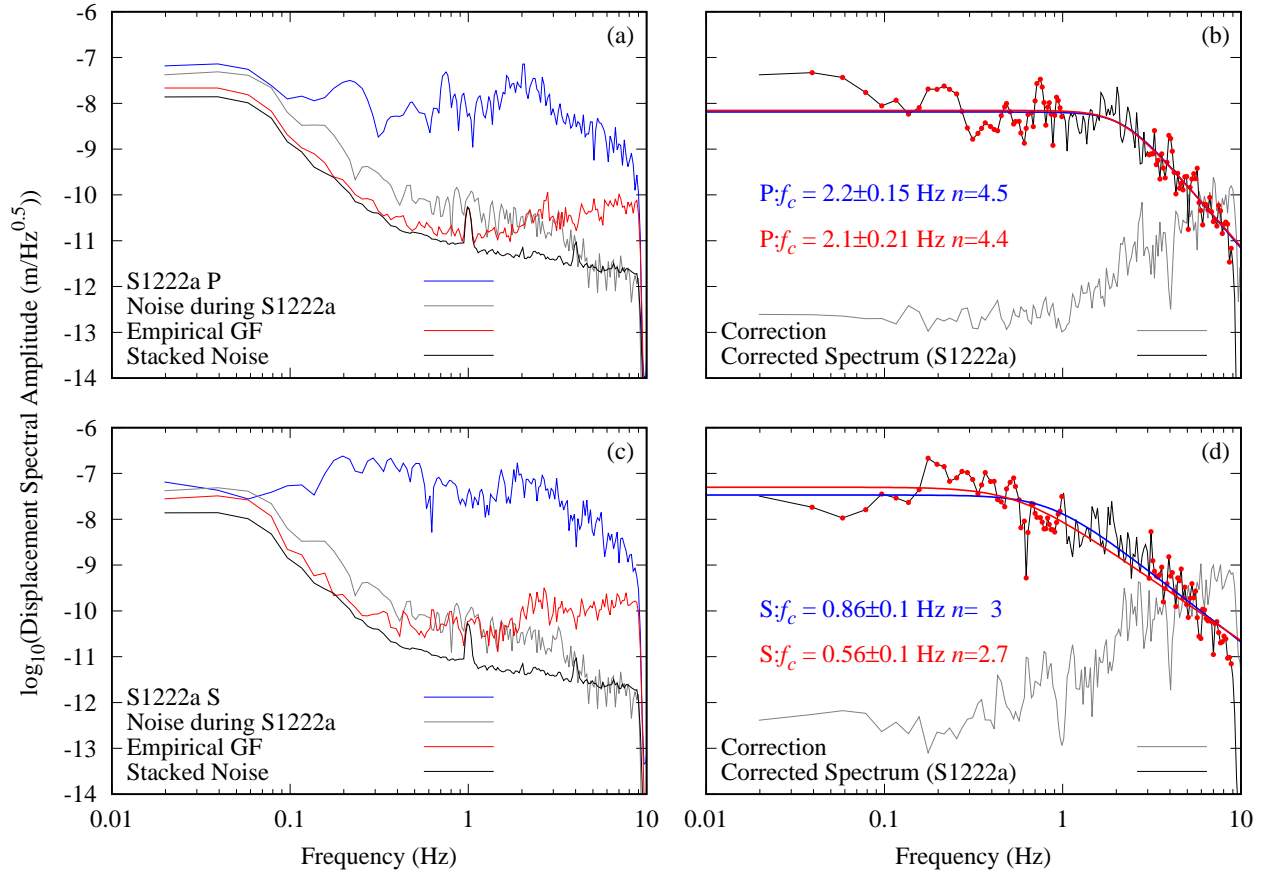


Figure S10. Empirical Green's Function (EGF) analyses performed for S1222a with general form of a source time function on transverse component $\gamma = 1$. We used the same setting as Figure 4 in the main text. Note that since not all events have their back azimuth estimated from the data, we took both N and E component and stacked to obtain the EGF and the stacked noise.

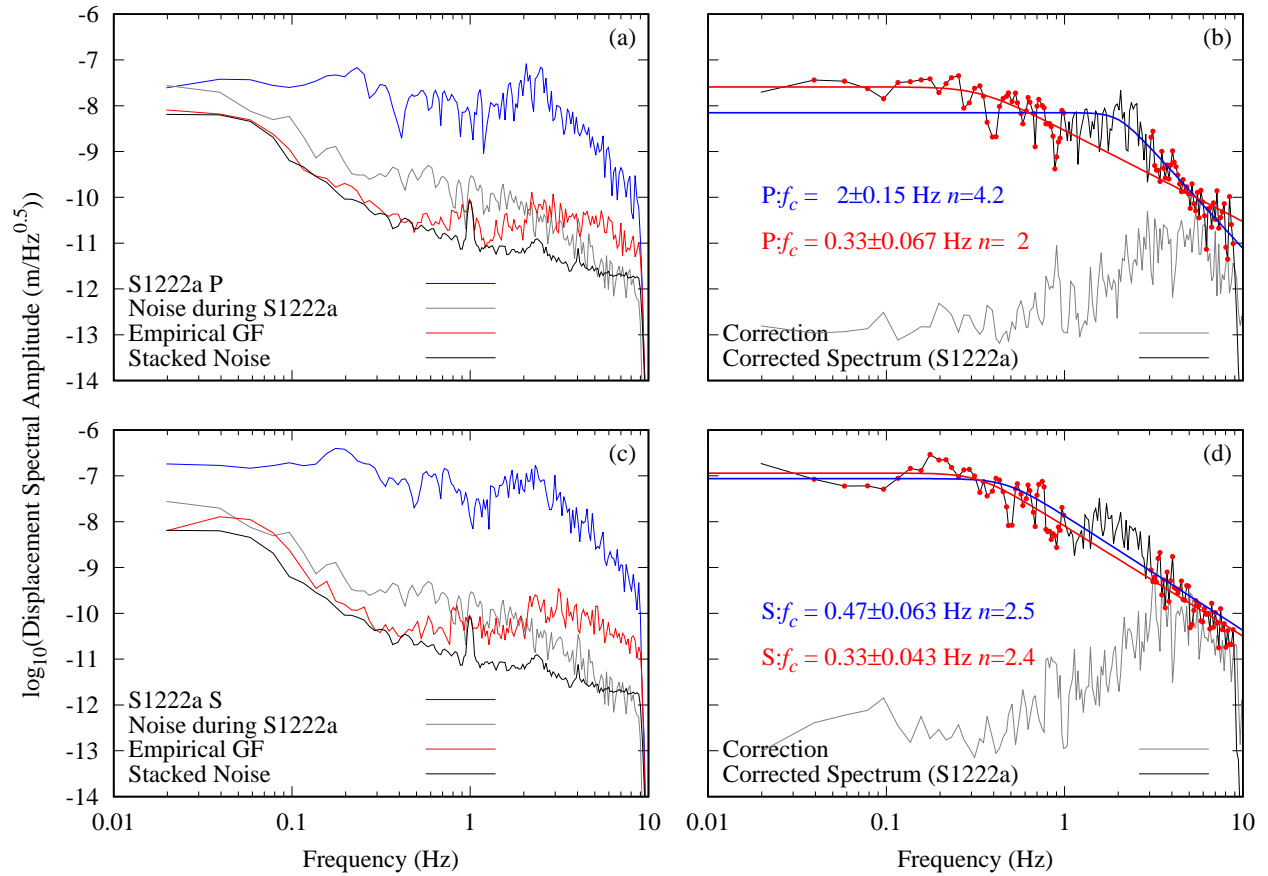


Figure S11. Empirical Green's Function (EGF) analyses performed for S1222a with general form of a source time function on vertical component $\gamma = 2$. We used the same setting as Figure 2 in the main text.

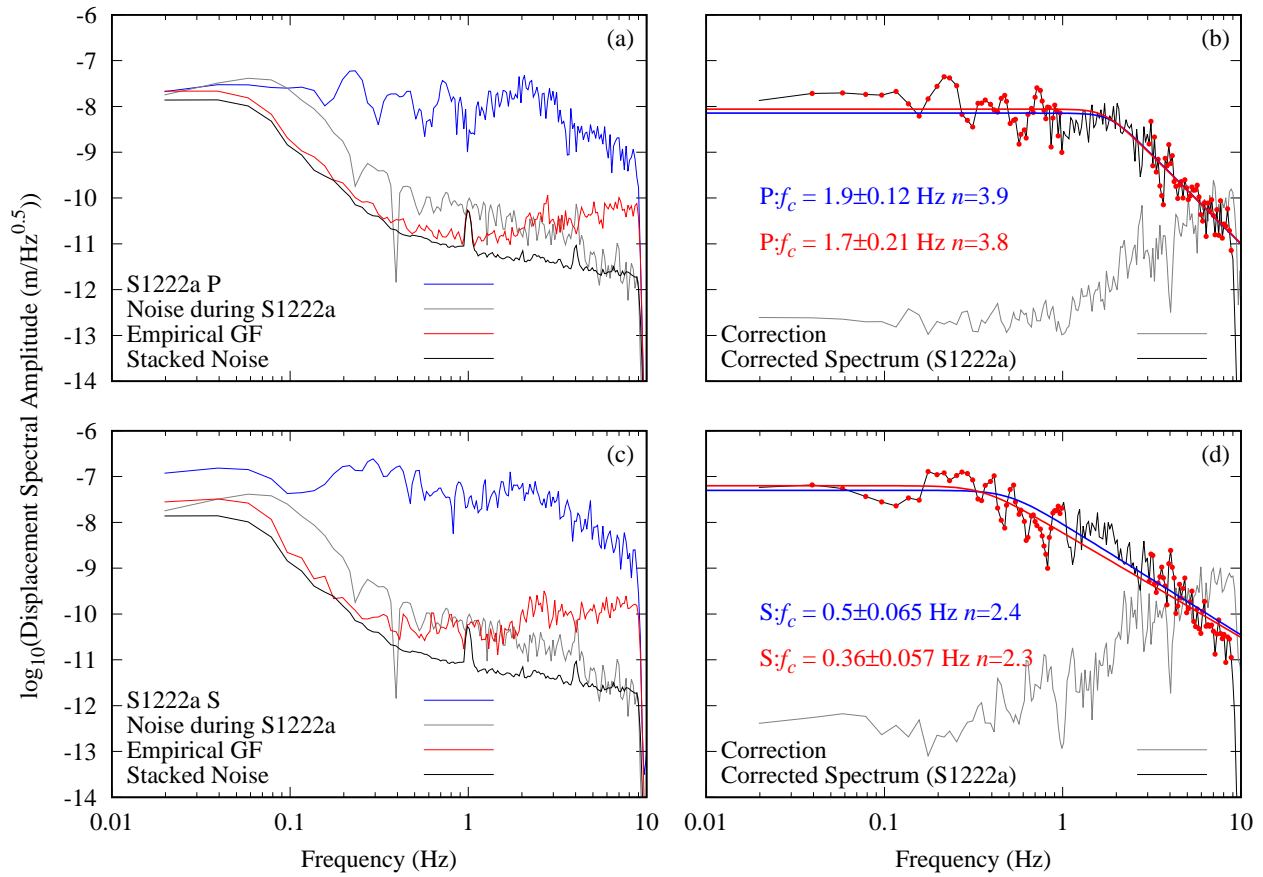


Figure S12. Empirical Green's Function (EGF) analyses performed for S1222a with general form of a source time function on radial component $\gamma = 2$. We used the same setting as Figure 2 in the main text. Note that since not all events have their back azimuth estimated from the data, we took both N and E component and stacked to obtain the EGF and the stacked noise.

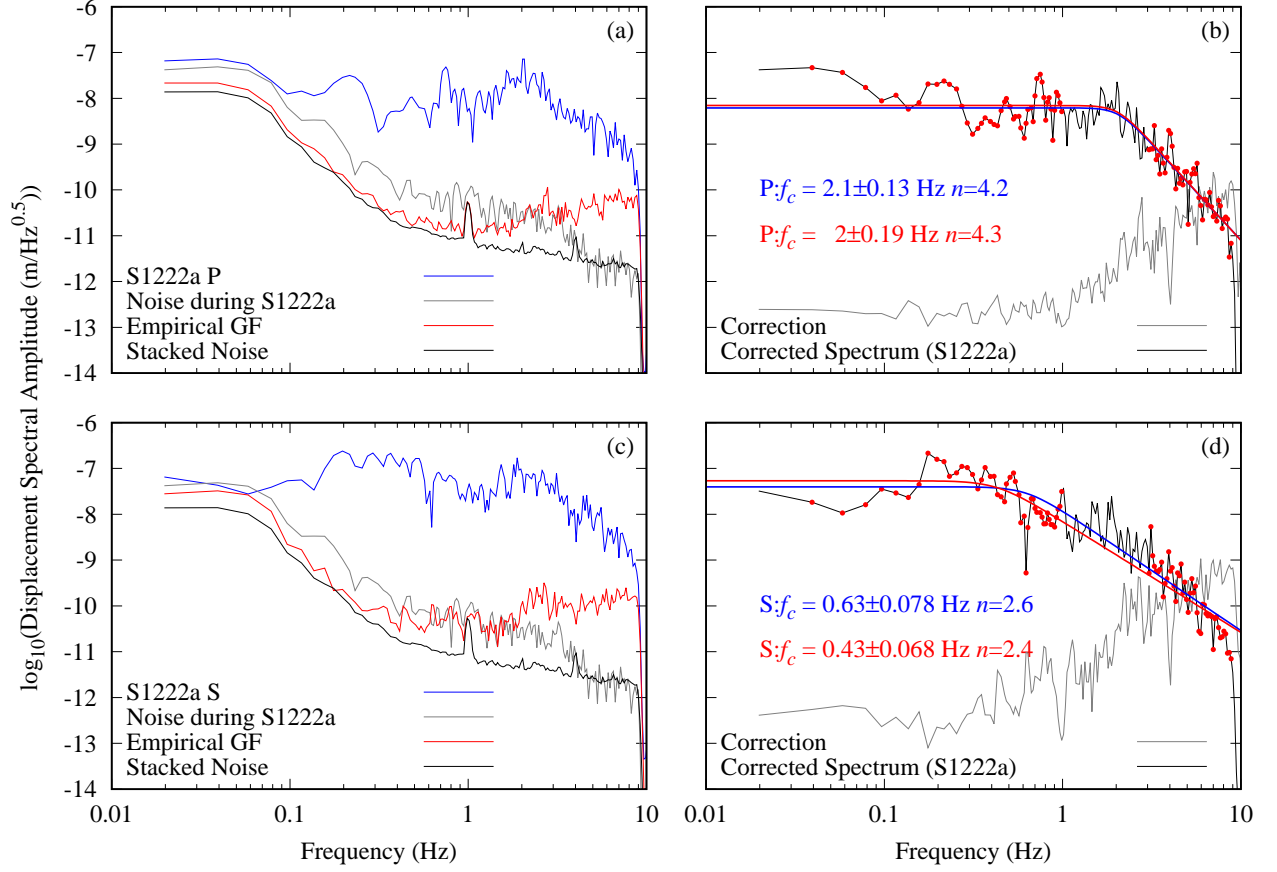


Figure S13. Empirical Green's Function (EGF) analyses performed for S1222a with general form of a source time function on transverse component $\gamma = 2$. We used the same setting as Figure 2 in the main text. Note that since not all events have their back azimuth estimated from the data, we took both N and E component and stacked to obtain the EGF and the stacked noise.